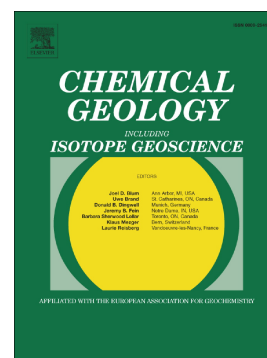


## Journal Pre-proof

An expanded shale  $\delta^{98}\text{Mo}$  record permits recurrent shallow marine oxygenation during the Neoproterozoic

Chadlin M. Ostrander, Brian Kendall, Stephanie L. Olson, Timothy W. Lyons, Gwyneth W. Gordon, Stephen J. Romaniello, Wang Zheng, Christopher T. Reinhard, Moutusi Roy, Ariel D. Anbar



PII: S0009-2541(19)30520-0

DOI: <https://doi.org/10.1016/j.chemgeo.2019.119391>

Reference: CHEMGE 119391

To appear in: *Chemical Geology*

Received date: 9 August 2019

Revised date: 7 November 2019

Accepted date: 11 November 2019

Please cite this article as: C.M. Ostrander, B. Kendall, S.L. Olson, et al., An expanded shale  $\delta^{98}\text{Mo}$  record permits recurrent shallow marine oxygenation during the Neoproterozoic, *Chemical Geology* (2018), <https://doi.org/10.1016/j.chemgeo.2019.119391>

This is a PDF file of an article that has undergone enhancements after acceptance, such as the addition of a cover page and metadata, and formatting for readability, but it is not yet the definitive version of record. This version will undergo additional copyediting, typesetting and review before it is published in its final form, but we are providing this version to give early visibility of the article. Please note that, during the production process, errors may be discovered which could affect the content, and all legal disclaimers that apply to the journal pertain.

© 2018 Published by Elsevier.

# An expanded shale $\delta^{98}\text{Mo}$ record permits recurrent shallow marine oxygenation during the Neoproterozoic

Chadlin M. Ostrander<sup>1\*</sup>, Brian Kendall<sup>2</sup>, Stephanie L. Olson<sup>3</sup>, Timothy W. Lyons<sup>4</sup>, Gwyneth W. Gordon<sup>1</sup>, Stephen J. Romaniello<sup>5</sup>, Wang Zheng<sup>6</sup>, Christopher T. Reinhard<sup>7</sup>, Moutusi Roy<sup>1</sup>, Ariel D. Anbar<sup>1,8</sup>

1. School of Earth and Space Exploration, Arizona State University, Tempe, AZ, USA
2. Department of Earth and Environmental Sciences, University of Waterloo, Waterloo, Ontario, Canada
3. Department of Geophysical Sciences, University of Chicago, Chicago, IL, USA
4. Department of Earth Sciences, University of California, Riverside, Riverside, CA, USA
5. Department of Earth and Planetary Sciences, University of Tennessee, Knoxville, TN, USA
6. Institute of Surface-Earth System Science, Tianjin University, Tianjin, China
7. School of Earth and Atmospheric Sciences, Georgia Institute of Technology, Atlanta, GA, USA
8. School of Molecular Science, Arizona State University, Tempe, AZ, USA

\*cmostran@asu.edu (corresponding author)

## Abstract:

Multiple attempts have been made using the ancient shale record to track the molybdenum isotope composition ( $\delta^{98}\text{Mo}$ ) of seawater during the final two-hundred million years of the Archean Eon (2.7 to 2.5 billion-years-ago, or Ga). This seawater  $\delta^{98}\text{Mo}$  value is important because it should have scaled with levels of ocean oxygenation during the runup to the Great Oxidation Event. Unfortunately, however, it is difficult to tell if the majority of the existing late-Archean shale  $\delta^{98}\text{Mo}$  record tracks an ancient seawater value. Here, we further attempt to track pre-GOE seawater  $\delta^{98}\text{Mo}$  using an expanded and well-characterized shale sample set from Western Australia (Jeerinah, Wittenoom, and Mt. Sylvia Formations) and South Africa (Nauga and Klein Naute Formations). Most importantly, and in contrast to most previous Mo isotope studies of similarly aged shales, local redox conditions for our shales have been independently constrained using the iron (Fe) speciation proxy. Local redox conditions are an important parameter because transfer of the seawater  $\delta^{98}\text{Mo}$  to sediments today is shown to be dependent on these conditions. According to our updated sedimentary  $\delta^{98}\text{Mo}$  record, seawater  $\delta^{98}\text{Mo}$  commonly exceeded 1.0‰ between ~2.69 Ga and 2.50 Ga. In order to drive such a heavy seawater  $\delta^{98}\text{Mo}$ , there must have been a marine sink with a strong preference for lighter-mass Mo isotopes frequently present over this

timeframe. The operation of some anaerobic processes in late-Archean marine settings could theoretically explain the heavier seawater  $\delta^{98}\text{Mo}$ . Such processes are known to promote the preferential retention of lighter-mass Mo isotopes in marine sediments today (e.g., interactions between Mo and organic matter or the formation of thio-complexes). Alternatively, or in addition, adsorption of lighter-mass Mo isotopes to Fe and Mn oxide minerals formed in oxygenated marine environments can explain the heavier seawater  $\delta^{98}\text{Mo}$ . A compilation of previous work suggests that oxygenated shallow marine environments were fairly common during the late-Archean, and thus Mo adsorption to Fe-Mn oxides formed in these settings probably played an important role in driving heavy seawater  $\delta^{98}\text{Mo}$  over this timeframe.

## 1. Introduction

A clearer picture of Earth's initial oxygenation is emerging. Molecular oxygen ( $\text{O}_2$ ) is still thought to have first accumulated in the atmosphere to appreciable levels between about 2.5 and 2.3 billion years ago (Ga), during what is referred to as the Great Oxidation Event (GOE; Bekker et al. 2004, Luo et al. 2016, Gumsley et al. 2017, Philippot et al. 2018). However, many recently discovered lines of evidence suggest that  $\text{O}_2$  had accumulated at Earth's surface in small amounts well before the GOE, perhaps as early as  $\sim 3.8$  Ga (summarized by Lyons et al. [2014]). Most likely, this early accumulation took place within oxygen "oases" near the sites of  $\text{O}_2$  production: on land within biological soil crusts (Konhauser et al. 2011, Lalonde and Konhauser 2014), in lacustrine benthic mats (Sumner et al. 2015), or in productive portions of shallow marine environments (Kasting 1992, Olson et al. 2013). Cyanobacteria in any of these locations could have produced  $\text{O}_2$  with minimal impact on global atmospheric oxygenation, keeping  $\text{O}_2$  levels in Earth's atmosphere very low until the GOE ( $p\text{O}_2 < 10^{-5}$  to  $10^{-7}$  the Present Atmospheric Level, or PAL [Farquhar et al. 2000, Pavlov and Kasting 2002, Zahnle et al. 2006]).

Multiple attempts have been made to track the oxygenation of Earth's shallow ocean during the runup to the GOE using molybdenum isotope compositions (reported in delta notation as  $\delta^{98}\text{Mo} = \{({}^{98/95}\text{Mo}_{\text{sample}} \div {}^{98/95}\text{Mo}_{\text{NIST SRM 3134}} - 1) \times 1000\} + 0.25\text{‰}$  [Nägler et al. 2014]) preserved in ancient marine shales (Wille et al. 2007, Duan et al. 2010, Eroglu et al. 2015, Kurzweil et al. 2015, Ostrander et al. 2019a). The  $\delta^{98}\text{Mo}$  of ancient seawater is generally thought to have scaled with levels of past ocean oxygenation (e.g., Arnold et al. 2004, Dahl et al. 2010, Chen et al. 2015). This idea arises from the fact that insoluble iron (Fe) and manganese (Mn) oxide minerals that can readily form in the presence of  $\text{O}_2$  preferentially sorb lighter-mass Mo isotopes (Wasylenki et al. 2008, Goldberg et al. 2009). When  $\text{O}_2$  initially accumulated in Earth's ocean, precipitation and deposition of these oxide minerals should have led to the preferential accumulation of heavier-mass Mo isotopes in seawater. This isotopically heavy seawater signature may be recorded as high  $\delta^{98}\text{Mo}$  in certain marine sedimentary rocks. Indeed, a few late-Archean-aged shales and carbonates have significantly heavier  $\delta^{98}\text{Mo}$  (up to  $\delta^{98}\text{Mo} = 1.77 \pm 0.15\text{‰}$

[Wille et al. 2007, Duan et al. 2010, Eroglu et al. 2015, Kurzweil et al. 2015, Ostrander et al. 2019a]) than bulk upper continental crust ( $\delta^{98}\text{Mo} = \sim 0.30\text{‰}$  to  $0.40\text{‰}$  [Greber et al. 2014, Voegelin et al. 2014, Willbold and Elliot 2017]) and suggest at least sporadic oxygenation of Earth's ocean in the runup to the GOE.

Unfortunately, however, it is extremely difficult to tell whether or not much of the current pre-GOE shale  $\delta^{98}\text{Mo}$  record tracks an ancient seawater signature. Transfer of the seawater  $\delta^{98}\text{Mo}$  value to marine sediments today is shown to be dependent on local redox conditions and bottom water Mo availability (summarized in Kendall et al. [2017]). In anoxic and  $\text{H}_2\text{S}$ -bearing settings, the formation of particle-reactive thiomolybdate species ( $\text{MoO}_{4-x}\text{S}_x^{2-}$ ) can result in efficient transfer of Mo from seawater into marine sediments (particularly when  $\text{H}_2\text{S}_{[\text{aq}]} \geq 11 \mu\text{M}$  [Helz et al. 1996, Erickson and Helz 2000]). When Mo removal from euxinic bottom waters to sediments in these environments is nearly quantitative, then the  $\delta^{98}\text{Mo}$  of the euxinic sediments is equal to the global seawater value—or nearly so. Today, these conditions are met in redox-stratified restricted basins where local bottom water Mo availability is low. In such cases, Mo removal to the underlying euxinic sediments together with slow deep-water exchange with the open ocean hinders Mo recharge to the local bottom waters (the Black Sea [Neubert et al. 2008], Kyllaren fjord [Noordmann et al. 2015], and Lake Rogoznica [Bura-Nakić et al. 2018]). Evidence for locally euxinic depositional conditions has been provided for only a few Archean-aged shales targeted to date for Mo isotope analyses (the 2.7 Ga Carajás Formation from Brazil [Cabral et al. 2013] and the 2.5 Ga Mt. McRae Shale from Western Australia [Duan et al. 2010, Ostrander et al. 2019a]). Furthermore, little is often known about bottom water Mo availability during deposition of these shales (despite established methods for qualitatively estimating this parameter; e.g., Mo/TOC ratios [Algeo and Lyons 2006]). Accordingly, it is difficult to tell whether or not much of the late-Archean shale  $\delta^{98}\text{Mo}$  record may track ancient seawater  $\delta^{98}\text{Mo}$ . By extension, it is then also difficult to track late-Archean ocean oxygenation using this record (a pitfall also elucidated by differences in the seawater  $\delta^{98}\text{Mo}$  estimates inferred from carbonates and shales from the same late-Archean strata [Voegelin et al. 2010]).

Here, we further attempt to track pre-GOE ocean oxygenation by applying the Mo isotope paleoredox proxy to an expanded set of well-characterized late-Archean-aged shales. We have measured the Mo isotope compositions of 140 ancient shale samples from drill core from Western Australia (from the Jeerinah, Wittenoom, and Mt. Sylvia Formations) and South Africa (from the Nauga and Klein Naute Formations) deposited between  $\sim 2.69$  Ga and 2.50 Ga. Critically, and unlike most previous Mo isotope studies of similarly-aged shales, local redox conditions for our shales have been independently constrained using the Fe speciation proxy. Moreover, bottom water Mo contents at the time of deposition for many of our shales have been qualitatively estimated using Mo/TOC ratios.

Iron speciation is an often-employed means for identifying ancient shales that were originally deposited under an euxinic water column (reviewed recently by Raiswell et al. [2018]). In short, much of the Fe is present in marine settings in the water column or as species that are reactive toward H<sub>2</sub>S on short, diagenetic timescales (e.g., dissolved Fe, carbonates, or oxides), and availability of this reactive Fe is typically elevated under anoxic depositional conditions. For a Precambrian shale to confidently qualify as being originally deposited under an anoxic water column, highly reactive Fe (Fe<sub>HR</sub>) needs to comprise more than 38% of its total Fe content (Fe<sub>HR</sub>/Fe<sub>T</sub> > 0.38 [Poulton and Canfield 2011]). Furthermore, the extent to which these highly reactive Fe-bearing minerals have been converted to pyrite is dependent on the presence or absence of H<sub>2</sub>S in the local water column (and perhaps also in sediment pore waters; see Hardisty et al. [2018]). As such, Fe as pyrite (Fe<sub>PY</sub>) needs to comprise at least 80% of the highly reactive Fe pool in an ancient shale for us to interpret the ancient depositional setting as euxinic (Fe<sub>PY</sub>/Fe<sub>HR</sub> > 0.80 [Poulton and Canfield 2011]).

A classic method for constraining ancient bottom-water Mo contents is by comparing the relative abundances of Mo and TOC in marine sedimentary rocks (Algeo and Lyons 2006). Ratios of Mo/TOC are high in sediments from modern euxinic basins that are well connected to the open ocean because Mo in the bottom waters of these basins is continually recharged (e.g., in the modern Cariaco Basin, where sedimentary Mo/TOC ratios average 25 ppm/wt% [Algeo and Lyons 2006]). In comparison, Mo/TOC are lower in sediments from modern anoxic basins with a poor connection to the open ocean because Mo recharge is comparatively muted (e.g., in the modern Black Sea, where sedimentary Mo/TOC ratios average 4.5 ppm/wt% [Algeo and Lyons 2006]). Accordingly, the relative availability of Mo in bottom waters of these basins is fingerprinted by their sedimentary Mo/TOC ratios—that is, a high sedimentary Mo/TOC ratio fingerprints elevated Mo contents in bottom waters, and vice-versa.

By targeting shales of known local depositional redox, and by also qualitatively assessing bottom water Mo availability, we are well positioned to differentiate shales that may have captured the coeval seawater δ<sup>98</sup>Mo signature during the late-Archean from those that probably did not. By extension, we are then also better prepared to track pre-GOE ocean oxygenation using the ancient shale record.

## 2. Shale samples

Figure 1 provides a generalized stratigraphy of the cores targeted in this study from the Pilbara Craton of Western Australia and the Kaapvaal Craton of South Africa, their approximate correlations, and highlights available age constraints. Neoproterozoic shales from these two locations are thought to have been deposited in the same marine basin along the active margin of a paleo-continent referred to as Vaalbara (de Kock et al. 2009). Our cores and their stratigraphy are described in detail in previous work (ABDP9:

Anbar et al. [2007], AIDP2 and AIDP3: Koehler et al. [2018], GKP01 and GKF01: Schröder et al. [2006]), and so we limit the details below to brief overviews.

## 2.1. Western Australia shales

### *The Jeerinah Formation (~2.69 – 2.63 Ga)*

Organic-rich shales of the Jeerinah Formation, often referred to as the Roy Hill Shale, from two cores recently drilled in Western Australia comprise the oldest rocks targeted in this study. The cores were drilled in the Pilbara Craton in 2012 as part of the Agouon Institute Drilling Program (AIDP) and have been designated as AIDP2 and AIDP3. Sites were chosen based on low regional metamorphism, and special care was taken to avoid drill contamination, specifically for the purpose of testing highly contentious Archean hydrocarbon biomarkers (French et al., 2015). Both cores intersect nearly 100m of continuous organic-rich and pyritic shale deposition. Shales in both cores are thought to have been deposited below storm wave base along a basinal depth gradient, with shales in AIDP2 being deposited closer to shore than those from AIDP3 (Koehler et al. 2018). The only precise time correlation between the two cores is an impact spherule bed, which occurs in AIDP2 near the bottom of the Carawine Dolomite and in AIDP3 during deposition of the upper Jeerinah Formation (Koehler et al. 2018). Age estimates derived from zircon U-Pb geochronology of volcanoclastics at the bottom and top of the Jeerinah Formation constrain deposition to a timeframe of about  $2.690 \pm 0.016$  Ga (Arndt et al. 1991) to  $2.629 \pm 0.005$  Ga (Trendall et al. 2004).

### *The Wittenoom and Mt. Sylvia Formations (~2.60 – 2.51 Ga)*

Shales of the Wittenoom and Mt. Sylvia formations used in this study come from drill core ABDP9, which was retrieved in the summer of 2004 as a part of the Archean Biosphere Drilling Project (ABDP). Sedimentary rocks preserved in the ABDP9 core have experienced only mild regional metamorphism (prehnite-pumpellyite faces to  $<300^{\circ}\text{C}$ ) and minimal deformation (gentle folding dips  $<5^{\circ}$ ) (Brocks et al. 2003). The dominant lithologies in the Wittenoom Formation from ABDP9 are carbonates and gray shales, but black shales occur between 350m and 330m core depth and are also interbedded with gray shales between 270m and 240m. Sedimentary rocks of the younger Mt. Sylvia Formation oscillate between black shales and banded iron formation. All sedimentary rocks targeted here from drill core ABDP9 are thought to have been deposited below storm wave base in an outer-shelf setting (Morris and Horwitz 1983). Zircon U-Pb ages of volcanoclastics from the underlying Marra Mamba Formation indicate that deposition of the Wittenoom Formation began after  $2.597 \pm 0.005$  Ga (Trendall et al. 1998), and zircon U-Pb ages for volcanoclastics within the Wittenoom Formation indicate that deposition ended sometime after  $2.565 \pm 0.009$  Ga (Trendall et al. 2004). Shales of the younger Mt. Sylvia Formation were

deposited after  $2.565 \pm 0.009$  Ga but before  $2.495 \pm 0.014$  Ga based on a Re-Os age constraint for deposition of the overlying Mt. McRae Shale (Kendall et al. 2015).

## 2.2. South Africa shales

### *The Nauga and Klein Naute Formations (>2.59 – 2.50 Ga)*

Shale samples from the Nauga and Klein Naute Formations come from two well-preserved and extensive drill cores from South Africa referred to as GKP01 and GKF01. Both cores were drilled as a part of the Agouron Drilling Project, and similar to the recently drilled AIDP cores, water was used as a lubricant to avoid organic contamination (Schröder et al. 2006). Post-depositional alteration is minimal in both cores and limited to gentle tectonic warping due to sub-greenschist facies metamorphism (Miyano and Beukes 1984). The dominant lithology in both cores is dolostone and microbialites, but organic-rich shales are present in intervals of both cores (Schröder et al. 2006). These shales include multiple discrete beds within the Nauga Formation (referred to, in order of decreasing age, as N1, N2, and N3 [Kendall et al. 2010]) and a comparatively more extensive occurrence in the Klein Naute Formation. Sedimentary rocks from drill core GKP01 are thought to have been deposited further from shore than those in GKF01 (slope-basin transition versus slope of the carbonate platform, respectively [Schröder et al. 2006]). The transition in both cores from carbonate-dominated deposition of the Nauga Formation to shale-dominated deposition recorded in the Klein Naute Formation was likely due to drowning of the carbonate platform in response to sea level rise (Schröder et al. 2006). Deposition of the Nauga Formation started earlier than  $2.588 \pm 0.006$  Ga (Altermann and Nelson 1998) and ended sometime after  $2.521 \pm 0.003$  Ga (Sumner and Bowring 1996) based on zircon U-Pb ages derived from volcanoclastics in the middle and upper parts of the formation, respectively. A lower age-limit for the Klein Naute Formation is  $2.480 \pm 0.006$  Ga based on a U-Pb age derived from a zircon in the overlying Kuruman Iron Formation (Nelson et al. 1999). A case has also been made that shales from the Klein Naute Formation may be coeval to shales of the Mt. McRae Shale from Western Australia (Kendall et al. 2010 and references therein). If this is correct, deposition of the Klein Naute Formation extended until at least  $2.495 \pm 0.014$  Ga (Kendall et al. 2015).

## 3. Analytical Methods

### 3.1. Fe speciation methods

Iron speciation data was obtained at the Department of Earth and Planetary Sciences at the University of California-Riverside using a calibrated sequential extraction protocol (Reinhard et al. 2009, Kendall et al. 2010). First, about 100 mg of shale sample powder were treated with a buffered sodium acetate solution (pH = 4.5) to extract carbonate-associated Fe ( $\text{Fe}_{\text{carb}}$ : siderite, ferroan calcite, or dolomite-ankerite solid solution series). Next, samples were treated with a buffered sodium dithionite solution (pH



= 4.8) to extract “reducible” Fe oxide phases that are reactive to hydrogen sulfide on early diagenetic timescales ( $\text{Fe}_{\text{OX}}$ : goethite and hematite). Samples were then treated with a 0.2M ammonium oxalate and 0.17M oxalic acid solution ( $\text{pH} = 3.2$ ) to extract magnetite ( $\text{Fe}_{\text{mag}}$ ). These sequential extractions were diluted 100x in trace metal grade 2% nitric acid and analyzed using an Agilent 7500cc ICP-MS. Replicate reproducibility was typically better than ~4%. Pyrite iron ( $\text{Fe}_{\text{PY}}$ ) was calculated (assuming a stoichiometry of  $\text{FeS}_2$ ) based on the wt% sulfur extracted during a two-hour hot chromous chloride distillation followed by iodometric titration. Replicate reproducibility for this step was typically below ~3%. Highly reactive iron ( $\text{Fe}_{\text{HR}}$ ) is defined as the sum of  $\text{Fe}_{\text{carb}} + \text{Fe}_{\text{OX}} + \text{Fe}_{\text{mag}} + \text{Fe}_{\text{PY}}$ .

In this study, new Fe speciation data are reported only for shales of the Wittenoom and Mt. Sylvia Formations. Iron speciation data were already published for the other shale units: the Jeerinah Formation in AIDP2 and AIDP3 (Olson et al. 2019) and the Nauga and Klein Naute Formations in GKP01 and GKF01 (Kendall et al. 2010).

### 3.2. Trace metal concentration methods

Trace metal concentration data were generated at the W.M. Keck Foundation Laboratory for Environmental Biogeochemistry, School of Earth and Space Exploration, Arizona State University (ASU). Whole-rock samples were powdered, ashed, and dissolved, and the resulting concentrations were analyzed using the methods outlined in Anbar et al. (2007). In short, powdered samples were ashed overnight in a muffled furnace at  $550^\circ\text{C}$  to help rid samples of organic material. Then, each sample was transferred to a trace metal clean lab and subjected to multiple rounds of concentrated acid digestion using trace metal grade hydrofluoric, hydrochloric, and nitric acid. Once completely dissolved, samples were diluted in 2% nitric acid and a few drops of HF in preparation for concentration analysis on a Thermo Scientific X-series quadrupole ICP-MS.

Trace metal concentrations were measured against multi-element calibration standards. Signal intensities for each analyte were at least three times greater than the blank and were bracketed by the least and most concentrated of these calibration standards. To correct for signal drift, an internal standard solution containing Ge, In, Y, and Bi was introduced in parallel with all samples and standards. Reproducibility for the analyte concentrations was better than 5% except for low Re samples (when Re concentrations are ~1.5 ng/g, the reproducibility drops to ~8%). USGS Geochemical Reference Materials SDO-1 (Devonian Shale) and SCO-1 (Cody Shale) were processed and measured alongside each set of samples to verify accuracy and were reproducible within error of published values.

New trace metal data is reported here only for shales of the Wittenoom and Mt. Sylvia Formations. Trace metal data were already published for the other shales: the Jeerinah Formation in



AIDP2 and AIDP3 (Olson et al. 2019) and the Nauga and Klein Naute Formations in GKP01 and GKF01 (Kendall et al. 2010).

### 3.3. Mo isotope methods

Isotope purification and analysis was also conducted at the W.M. Keck Foundation Laboratory at ASU following procedures outlined in previous work (Ostrander et al., 2019a, and references therein). In brief, enough sample was taken from stock solutions to provide 125 ng of Mo, followed by double-spiking with synthetic Mo ( $^{97}\text{Mo}$  and  $^{100}\text{Mo}$ ) prior to purification via ion exchange chromatography (Barling et al. 2001). After the sample matrix was removed, isotope ratio measurements were performed on a Thermo Neptune multi-collector ICPMS (MC-ICPMS) in low-resolution mode utilizing sample-standard bracketing and double spike analysis to correct for instrumental mass bias. Both samples and standards were analyzed at a concentration of 25 ng/g Mo, which yielded typically around three volts of signal on mass 98. Individual sample solutions were analyzed in duplicate at least, but the overwhelming majority were analyzed in triplicate.

Average 2SD sample reproducibility was 0.05‰, and the maximum was 0.17‰. All measurements were made relative to the Johnson Matthey Specpure Mo plasma standard (Lot #802309E; RochMo2) and then recalculated relative to the international NIST SRM 3134 standard set to + 0.25‰ (Nägler et al., 2014). In brief, the measured value for NIST SRM 3134 during our analytical sessions was  $0.33 \pm 0.03\text{‰}$  (2SD) relative to RochMo2 (Table 1). Accordingly, 0.08‰ was subtracted from each sample measured relative to RochMo2 to yield the sample isotope composition relative to NIST SRM 3134 = +0.25‰. USGS rock reference material SDO-1 was simultaneously processed with each batch of samples to monitor accuracy and showed good reproducibility ( $1.01 \pm 0.10\text{‰}$  [2SD, n = 21] compared to a multi-laboratory average of  $1.05 \pm 0.14\text{‰}$  [2SD] from Goldberg et al. 2013), as did various sample solutions (Table 1). Reported errors for our samples are always in 2SD and either equal to the 2SD reproducibility of the SDO-1 powder processed alongside our samples (0.10‰; noted above) or the individual sample's reproducibility, whichever is greater. For each analytical run, we measured a series of standards with varying spike-sample ratios. All samples were within the validated spike-sample range for accurate and precise  $\delta^{98}\text{Mo}$  measurements.

**Table 1. Mo isotope data from standard reference material solutions**

Standard	$\delta^{98}\text{Mo}^{\text{a}}$	N	Normalized to NIST + 0.25‰	Goldberg et al. (2013)
ICL-Mo	$0.16 \pm 0.03\text{‰}$	36	$0.08 \pm 0.03\text{‰}$	$0.09 \pm 0.05\text{‰}$
Kyoto-Mo	$-0.05 \pm 0.05\text{‰}$	36	$-0.13 \pm 0.05\text{‰}$	$-0.12 \pm 0.06\text{‰}$
NIST SRM 3134	$0.33 \pm 0.03\text{‰}$	41	0.25‰	0.25‰
SDO-1	$1.13 \pm 0.05\text{‰}$	41	$1.05 \pm 0.05\text{‰}$	$1.05 \pm 0.14\text{‰}$

a. measured relative to Roch-Mo2

\*all reported errors are 2SD of the standard reproducibility

## 4. Results

In addition to highlighting the results of our study, we also recap in this section pertinent Fe speciation and elemental concentration data reported in previous studies of the same shale samples.

### 4.1. Data from shales of the Jeerinah Formation

Iron speciation data from the Jeerinah Formation in drill cores AIDP2 and AIDP3 were recently reported by Olson et al. (2019) (Fig. 2). Instances of elevated  $\text{Fe}_{\text{HR}}/\text{Fe}_{\text{T}}$  and  $\text{Fe}_{\text{Py}}/\text{Fe}_{\text{HR}}$  ratios are present in both drill cores. For example,  $\text{Fe}_{\text{HR}}/\text{Fe}_{\text{T}} \geq 0.38$  and  $\text{Fe}_{\text{Py}}/\text{Fe}_{\text{HR}} \geq 0.80$  (ratios that can be ascribed confidently to local euxinia [Poulton and Canfield 2011]) are found in most Jeerinah shales from AIDP2 between 374.67m and 342.74m. Similar ratios are found in all shales from the AIDP3 drill core between 101.77m and 78.56m. Outside of these intervals, the majority of shale samples from both drill cores have lower  $\text{Fe}_{\text{HR}}/\text{Fe}_{\text{T}}$  and  $\text{Fe}_{\text{Py}}/\text{Fe}_{\text{HR}}$  ratios suggestive of ferruginous conditions.

Molybdenum concentration data were also recently reported for these shales, ranging from as low as 1  $\mu\text{g/g}$  to as high as 10  $\mu\text{g/g}$  (Olson et al. 2019; Fig. 2). In general, Mo abundances were found to be greater in the AIDP2 drill core when  $\text{Fe}_{\text{HR}}/\text{Fe}_{\text{T}}$  and  $\text{Fe}_{\text{Py}}/\text{Fe}_{\text{HR}}$  ratios were elevated (between 374.67m and 342.74m). This observation was not the case in AIDP3, however, as Mo abundances in this drill core were generally higher when  $\text{Fe}_{\text{Py}}/\text{Fe}_{\text{HR}} < 0.80$ .

Bulk-rock  $\delta^{98}\text{Mo}$  compositions measured by us in shales from the Jeerinah Formation range from  $-0.25 \pm 0.10\text{‰}$  to  $1.02 \pm 0.10\text{‰}$  (Fig. 2). The heaviest shale  $\delta^{98}\text{Mo}$  in both drill cores are within error of one another ( $0.98 \pm 0.10\text{‰}$  in AIDP2 and  $1.02 \pm 0.10\text{‰}$  in AIDP3), and both occur when  $\text{Fe}_{\text{HR}}/\text{Fe}_{\text{T}}$  is  $\geq 0.38$  and  $\text{Fe}_{\text{Py}}/\text{Fe}_{\text{HR}}$  is  $\geq 0.80$ . Overall,  $\delta^{98}\text{Mo}$  in shales from AIDP2 are heavier when Fe speciation ratios are elevated (between 374.67m and 342.74m, where the average  $\delta^{98}\text{Mo} = 0.85 \pm 0.31\text{‰}$ ). Molybdenum isotope compositions are comparatively lighter outside of this interval, peaking at  $0.69 \pm 0.10\text{‰}$  at 377.89m and averaging  $0.53 \pm 0.25\text{‰}$ . In comparison, the relationship between  $\delta^{98}\text{Mo}$  and Fe speciation data in shales from AIDP3 is less obvious. For example, heavy  $\delta^{98}\text{Mo}$  values are found in AIDP3 shales

with elevated Fe speciation ratios (e.g.,  $1.02 \pm 0.10\%$  at 68.22m) as well in shales with lower Fe speciation ratios (e.g.,  $0.82 \pm 0.10\%$  at 130.17m). Relatively light  $\delta^{98}\text{Mo}$  are also found in AIDP3 when  $\text{Fe}_{\text{HR}}/\text{Fe}_{\text{T}}$  and  $\text{Fe}_{\text{Py}}/\text{Fe}_{\text{HR}}$  are elevated (e.g.,  $0.25 \pm 0.10\%$  at 101.77m) as well as when they are low (e.g.,  $-0.25 \pm 0.10\%$  at 74.10m).

#### 4.2. Data from shales of the Wittenoom and Mt. Sylvia Formations

Our Fe speciation ratios generated for shales of the Wittenoom and Mt. Sylvia Formations from drill core ABDP9 are generally low (Fig. 3). Only one shale sample from these formations has  $\text{Fe}_{\text{HR}}/\text{Fe}_{\text{T}}$  of  $\geq 0.38$  and  $\text{Fe}_{\text{Py}}/\text{Fe}_{\text{HR}}$  of  $\geq 0.80$  (at 209.67m in the Mt. Sylvia Formation). There is a slight increase in  $\text{Fe}_{\text{HR}}/\text{Fe}_{\text{T}}$  and  $\text{Fe}_{\text{Py}}/\text{Fe}_{\text{HR}}$  ratios toward the top of the Wittenoom Formation, starting at 235.71m core depth. Above this depth and throughout the Mt. Sylvia Formation,  $\text{Fe}_{\text{HR}}/\text{Fe}_{\text{T}}$  is commonly greater than 0.38. No samples below 235.71m possess  $\text{Fe}_{\text{HR}}/\text{Fe}_{\text{T}}$  ratios of  $\geq 0.38$ .

Our Mo concentrations range from 1  $\mu\text{g/g}$  to 5  $\mu\text{g/g}$  in shales from the Wittenoom and Mt. Sylvia formations (Fig. 3). The only stratigraphic trend in Mo abundances occurs at 253.99m core depth, where  $\text{Fe}_{\text{HR}}/\text{Fe}_{\text{T}}$  and  $\text{Fe}_{\text{Py}}/\text{Fe}_{\text{HR}}$  both increase slightly. Above this depth, Mo abundances dip to as low as 1  $\mu\text{g/g}$ . Such low Mo abundances are not seen lower in the section.

Molybdenum isotope compositions range from  $0.57 \pm 0.10\%$  to  $1.44 \pm 0.10\%$  in shales from the Wittenoom and Mt. Sylvia formations (Fig. 3). The two heaviest  $\delta^{98}\text{Mo}$  values occur in shales from the younger Mt. Sylvia Formation ( $1.20 \pm 0.10\%$  at 218.91m and  $1.44 \pm 0.10\%$  at 197.00m), with the heavier of these two coming from our uppermost shale sample in ABDP9. For comparison, the heaviest  $\delta^{98}\text{Mo}$  from the Wittenoom Formation is  $1.03 \pm 0.10\%$  at 284.57m. Outside of these few heavy isotope compositions, the remainder of the  $\delta^{98}\text{Mo}$  in both formations are isotopically lighter and fairly invariant (average  $\delta^{98}\text{Mo} = 0.75 \pm 0.22\%$ ).

#### 4.3. Data from shales of the Nauga Formation

Kendall et al. (2010) and Zerkle et al. (2012) previously reported Fe speciation data for the shales in the Nauga Formation from drill cores GKP01 and GKF01 (Figs. 4 and 5). Between the two drill cores, only a single shale sample from GKP01 in the lowermost N1 interval of the Nauga Formation showed  $\text{Fe}_{\text{HR}}/\text{Fe}_{\text{T}}$  of  $\geq 0.38$  and  $\text{Fe}_{\text{Py}}/\text{Fe}_{\text{HR}}$  of  $\geq 0.80$  (639.20m core depth).

Molybdenum abundances in Nauga shales from GKP01 and GKF01 are persistently low in all sampling intervals, peaking at 3  $\mu\text{g/g}$  (Figs. 4 and 5). The lowest Mo concentrations from any shale units targeted in this study come from N1 in the Nauga Formation, with values as low as 0.2  $\mu\text{g/g}$  in GKF01.

Molybdenum abundances increase slightly in the younger shales, eclipsing 2  $\mu\text{g/g}$  for the first time in the N2 and N3 intervals of both cores.

Molybdenum isotope compositions in Nauga shales reported here are also persistently low in both drill cores, spanning a restricted range from  $0.10 \pm 0.10\text{‰}$  to  $0.38 \pm 0.10\text{‰}$  (Figs. 4 and 5). The lowest  $\delta^{98}\text{Mo}$  value comes from the N2 interval of GKF01 (625.18m). The heaviest  $\delta^{98}\text{Mo}$  comes from the N3 interval of GKF01 (439.64m). Of the seven total shale samples in the Nauga Formation with  $\delta^{98}\text{Mo}$  between 0.30‰ and 0.38‰, six are from this N3 interval in GKF01.

#### 4.4. Data from shales of the Klein Naute Formation

Iron speciation and trace metal data were also reported by Kendall et al. (2010) for the Klein Naute Formation shales targeted here from drill cores GKP01 and GKF01 (Figs. 4 and 5). Both drill cores have extended intervals of Klein Naute shale deposition where  $\text{Fe}_{\text{HR}}/\text{Fe}_{\text{T}}$  is  $\geq 0.38$  and  $\text{Fe}_{\text{Py}}/\text{Fe}_{\text{HR}}$  is  $\geq 0.80$ . In GKP01, these elevated Fe speciation ratios are found in many samples between 321.10m and 305.34m. In GKF01, similarly elevated Fe speciation ratios are found in many samples between 284.00m and 264.43m. Outside of these depth ranges in both cores,  $\text{Fe}_{\text{HR}}/\text{Fe}_{\text{T}}$  ratios often eclipse 0.38, but  $\text{Fe}_{\text{Py}}/\text{Fe}_{\text{HR}}$  never again exceeds 0.80.  $\text{Fe}_{\text{Py}}/\text{Fe}_{\text{HR}}$  are especially low in GKP01 between 292.50m and 248.00m, never exceeding 0.10.

Molybdenum abundances are highest in shales from the Klein Naute Formation compared to any of the other shale units we targeted, reaching values as high as 22  $\mu\text{g/g}$  in GKF01 (at 272.71m as reported in Kendall et al. [2010]; Figs. 4 and 5). In GKF01, high Mo abundances are found primarily in shales with elevated Fe speciation ratios (i.e., between 284.00m and 264.43m). The highest Mo abundances in GKP01 are also found primarily in shales with elevated Fe speciation ratios (i.e., between 321.10m and 305.34m). However, Mo abundances in GKP01 are not as high as those in GKF01, reaching only 8.6  $\mu\text{g/g}$  (312.73m).

Molybdenum isotope compositions in shales from the Klein Naute Formation span a wide range, from as low as  $0.38 \pm 0.10\text{‰}$  to as high as  $1.54 \pm 0.11\text{‰}$  (Figs. 4 and 5). Values for  $\delta^{98}\text{Mo}$  are generally heavier in GKF01 compared to GKP01. For example, the heaviest observed  $\delta^{98}\text{Mo}$  from both drill cores is from GKF01 ( $1.54 \pm 0.11\text{‰}$  at 274.23m core depth). In GKP01, the heaviest  $\delta^{98}\text{Mo}$  value is  $1.27 \pm 0.10\text{‰}$  (at 315.85m core depth). Furthermore, only one shale sample of the fourteen we measured for the Klein Naute Formation in GKF01 has a  $\delta^{98}\text{Mo}$  lower than 1.0‰ ( $0.89 \pm 0.12\text{‰}$  at 265.67m core depth). In GKP01, half of the shale samples we measured (10 out of 20) have  $\delta^{98}\text{Mo}$  values lower than 1.0‰. Of note, the heaviest  $\delta^{98}\text{Mo}$  value for GKF01 comes from a shale sample with a  $\text{Fe}_{\text{HR}}/\text{Fe}_{\text{T}}$  ratio of  $\geq 0.38$  and  $\text{Fe}_{\text{Py}}/\text{Fe}_{\text{HR}} \geq 0.80$ . In GKP01, the heaviest  $\delta^{98}\text{Mo}$  is *not* found in a shale sample with Fe speciation ratios that meet or exceed these thresholds. However, this sample is located within the interval of shales in

GKP01 where  $Fe_{HR}/Fe_T$  and  $Fe_{Py}/Fe_{HR}$  often exceed 0.38 and 0.80, respectively (between 321.10m and 305.34m). The three lightest  $\delta^{98}Mo$  values in the Klein Naute Formation (0.38‰ to 0.64‰) are from shales in GKP01 with especially low  $Fe_{HR}/Fe_T$  and  $Fe_{Py}/Fe_{HR}$  ratios (<0.38 and < 0.10, respectively, between 292.50m and 248.00m).

## 5. Discussion

In the following section we begin by discussing the influence of detrital contamination (**Section 5.1.**) and local redox conditions (**Section 5.2.**) on our shale  $\delta^{98}Mo$  data. Guided by our new data, we then estimate the seawater  $\delta^{98}Mo$  values between ~2.69 Ga and 2.50 Ga (**Section 5.3.**). This text is followed by a discussion of the links connecting our seawater  $\delta^{98}Mo$  estimates to pre-GOE ocean oxygenation (**Section 5.4.**).

### 5.1. Impact of detrital contamination on $\delta^{98}Mo$

It is evident that the extent of detrital Mo contamination played a key role in governing the  $\delta^{98}Mo$  of our late Archean shales. When shale  $\delta^{98}Mo$  are cross-plotted against Mo/Al for the same samples, a general logarithmic correlation is revealed ( $R^2 = 0.65$ ; Fig. 6). This correlation most likely fingerprints binary mixing in our samples between two distinct Mo sources. One of these sources had a low Mo/Al ratio and a light  $\delta^{98}Mo$ , each comparable to recent estimates for the modern upper continental crust (Mo/Al = 0.13 ppm/wt% [Rudnick and Gao 2003] and  $\delta^{98}Mo = \sim 0.30\%$  to  $0.40\%$  [Greber et al. 2014, Voegelin et al. 2014, Willbold and Elliot 2017]). Because Earth's upper continental crust is what eventually becomes detrital material, this first source was probably detritus. The other source had a much higher Mo/Al ratio and a heavier  $\delta^{98}Mo$  and was most likely seawater-derived (authigenic) Mo. It is reasonable to assume, since this correlation is found in shales deposited over ~200 million years, that the  $\delta^{98}Mo$  of both of these Mo sources was fairly constant over this timeframe. Thus, our measured bulk-shale  $\delta^{98}Mo$  was probably set primarily by the relative contribution from each (and to some extent also local depositional redox; see **Section 5.2.**).

*For the remainder of the text, we will discuss calculated authigenic  $\delta^{98}Mo$  contributions to our shale samples and not the detritally contaminated bulk-rock  $\delta^{98}Mo$ .* The fraction of Mo derived from detrital material ( $f_{detrital}$ ) for any shale sample can be estimated by:

$$f_{detrital} = (Al_{shale} \times Mo/Al_{detrital})/Mo_{shale}, \quad (1),$$

where  $Mo_{shale}$  signifies the Mo abundances measured in our bulk-shale samples, and  $Mo/Al_{detrital}$  represents the Mo/Al ratio of detrital material (assumed here to be equal to that of the upper continental

crust: 0.13 ppm/wt% [Rudnick and Gao 2003]). Then, the authigenic  $\delta^{98}\text{Mo}$  contribution ( $\delta^{98}\text{Mo}_{\text{authigenic}}$ ) can be estimated by;

$$\delta^{98}\text{Mo}_{\text{authigenic}} = [\delta^{98}\text{Mo}_{\text{shale}} - \delta^{98}\text{Mo}_{\text{detrital}} \times f_{\text{detrital}}] / 1 - f_{\text{detrital}}, \quad (2),$$

where  $\delta^{98}\text{Mo}_{\text{shale}}$  and  $\delta^{98}\text{Mo}_{\text{detrital}}$  signify the bulk-shale and detrital Mo isotope compositions, respectively. Here, we assume  $\delta^{98}\text{Mo}_{\text{detrital}}$  was 0.25‰ because this is the value extrapolated from our shale dataset in Fig. 6 when Mo/Al is assumed to be 0.13 (the most recent estimate for the bulk upper continental crust [Rudnick and Gao 2003]). Although our detrital  $\delta^{98}\text{Mo}$  estimate is slightly lighter than recent estimates for the modern upper continental crust ( $\delta^{98}\text{Mo} = \sim 0.30\text{‰}$  to  $0.40\text{‰}$  [Greber et al. 2014, Voegelin et al. 2014, Willbold and Elliot 2017]), it is in general agreement with a value extrapolated from detrital-rich late Archean shales from drill cores GKP01 and GKF01 analyzed in another study ( $0.20\text{‰}$  [Wille et al. 2007]). Furthermore, it is reasonable to assume that Archean continental crust had a greater proportion of mafic and ultramafic rocks with comparatively light  $\delta^{98}\text{Mo}$  ( $\delta^{98}\text{Mo} = \sim 0.05\text{‰}$  [Greber et al. 2015, McCoy-West et al. 2019]).

Notably, we do not calculate  $\delta^{98}\text{Mo}_{\text{authigenic}}$  values for shales with  $f_{\text{detrital}} \geq 0.60$ . We choose to impose this “detrital cutoff” because calculated  $\delta^{98}\text{Mo}_{\text{authigenic}}$  values for shales with such high  $f_{\text{detrital}}$  become particularly dependent on  $\delta^{98}\text{Mo}_{\text{detrital}}$  and Mo/Al<sub>detrital</sub>. This dependence is illustrated in Figure 7 and expanded upon below. It is reasonable to assume that detrital source rocks during the Archean possessed  $\delta^{98}\text{Mo}$  between that of komatiites ( $\sim 0.05\text{‰}$  [Greber et al. 2015, McCoy-West et al. 2019]) and the maximum estimated value for upper continental crust ( $\sim 0.40\text{‰}$  [Greber et al. 2014, Voegelin et al. 2014, Willbold and Elliot 2017]). When  $\delta^{98}\text{Mo}_{\text{authigenic}}$  is calculated for each of our shale samples using these endmember  $\delta^{98}\text{Mo}_{\text{detrital}}$ , the correction applied to our shales (that is, the difference between the calculated authigenic value and the measured shale value, or  $\Delta^{98}\text{Mo}_{\text{authigenic-shale}}$ ) becomes especially variable above  $f_{\text{detrital}} \sim 0.80$  (differences in  $\Delta^{98}\text{Mo}_{\text{authigenic-shale}} > 3.0\text{‰}$  between the separate  $\delta^{98}\text{Mo}_{\text{detrital}}$ ; Fig.7, upper panel). Likewise, detrital source rocks during the Archean probably possessed Mo/Al (in ppm/wt%) between that of the upper continental crust (0.09 [Wedepohl 1995] to 0.13 [Rudnick and Gao 2003]) and komatiites ( $\sim 0.18$ , based on a recent study of Archean komatiites from multiple cratons [Sossi et al. 2016]). When  $\delta^{98}\text{Mo}_{\text{authigenic}}$  are calculated using the plausible Mo/Al<sub>detrital</sub> endmembers, the corrections become especially variable above  $f_{\text{detrital}} \sim 0.60$  (differences in  $\Delta^{98}\text{Mo}_{\text{authigenic-shale}} > 6.0\text{‰}$  between the separate Mo/Al<sub>detrital</sub>; Fig. 7, lower panel). The only scenario that results in highly variable  $\Delta^{98}\text{Mo}_{\text{authigenic-shale}}$  with  $f_{\text{detrital}} < 0.60$  is one in which  $\delta^{98}\text{Mo}_{\text{detrital}}$  was equal to komatiites ( $0.00\text{‰}$ ) and Mo/Al<sub>detrital</sub> was equal to a lower-limit estimate for the modern upper continental crust (0.09) (scenario not plotted in Fig. 7). Because this pairing is unlikely, we think our  $f_{\text{detrital}} < 0.60$  cutoff is reasonable.



## 5.2. Impacts of local redox conditions on shale $\delta^{98}\text{Mo}$

### 5.2.1. Shales deposited under locally euxinic conditions

Shales of the Jeerinah and Klein Naute formations were at times deposited under at least locally euxinic conditions (signified by  $\text{Fe}_{\text{HR}}/\text{Fe}_{\text{T}} \geq 0.38$  and  $\text{Fe}_{\text{Py}}/\text{Fe}_{\text{HR}} \geq 0.80$  [Poulton and Canfield 2011]). Hence, by analogy with modern settings (Barling et al. 2001, Neubert et al. 2008, Noordmann et al. 2015, Bura-Nakić et al. 2018), these shales are our best candidates to have captured ancient seawater  $\delta^{98}\text{Mo}$  values. Just because Fe speciation data in these late-Archean shales suggests local deposition was euxinic, however, does not necessarily mean that transfer of the seawater  $\delta^{98}\text{Mo}$  to sediments definitely took place. For various reasons in euxinic settings today (e.g., insufficient  $\text{H}_2\text{S}$  and/or an overabundance of Mo in local bottom waters), quantitative transfer of Mo to sediments does not occur, along with incomplete conversion to thio-complexes. The result is sedimentary  $\delta^{98}\text{Mo}$  that are isotopically lighter than the seawater value (e.g.,  $\Delta^{98}\text{Mo}_{\text{seawater-sediment}} = < 0.5\text{‰}$  in strongly euxinic settings [Nägler et al. 2011, Bura-Nakić et al. 2018] and  $\Delta^{98}\text{Mo}_{\text{seawater-sediment}} = 0.5 - 3.0\text{‰}$  in weakly euxinic settings [Arnold et al. 2004, Neubert et al. 2008]). In this subsection, we discuss some reasons to be optimistic about the capture of ancient seawater  $\delta^{98}\text{Mo}$  in these shales and some others that are less encouraging.

There is reason to think that bottom-water Mo contents were low when deposition of shales from the Jeerinah and Klein Naute formations occurred under a euxinic water column, and this scenario would have helped promote transfer of seawater  $\delta^{98}\text{Mo}$  to sediments. Ratios of Mo/TOC in shales from the Jeerinah (up to 1.1 ppm/wt%) and Klein Naute (up to 3.3 ppm/wt%) formations deposited under euxinic conditions are lower than those found in sediments from the modern Black Sea (4.5 ppm/wt% [Algeo and Lyons 2006]). Thus, it is possible that bottom-water Mo concentrations at the original depositional sites for our euxinic shale samples from the Jeerinah and Klein Naute formations – and perhaps even in the worldwide ocean (Scott et al. 2008) – were predominantly very low, perhaps lower than those found in bottom waters of the modern Black Sea ( $< 10$  nM [Nägler et al. 2011]). If so, transfer of the seawater  $\delta^{98}\text{Mo}$  to these sediments was plausible, particularly if bottom-water sulfide concentrations were high.

On the other hand, there is also reason to imagine that only weakly or unstable euxinic conditions developed during deposition of some shales from the Jeerinah Formation, a scenario that could have hindered transfer of the seawater  $\delta^{98}\text{Mo}$  to these shales. A case was made in Olson et al. (2019), based on a general correlation between Mo and S abundances in shales from the Jeerinah Formation in drill core AIDP2, that Mo delivery to the original sediments was limited by low or unstable sulfide availability. In modern marine settings where localized euxinia is weak or unstable, quantitative transfer of Mo from seawater to sediments does not occur and leads to sedimentary  $\delta^{98}\text{Mo}$  that are always lighter than the



seawater value (e.g., Neubert et al. 2008, Nägler et al. 2011, Noordmann et al. 2015). More specifically, the formation and persistence of intermediate thiomolybdates ( $\text{MoO}_{4-x}\text{S}_x^{2-}$ ) in modern settings with low or variable  $\text{H}_2\text{S}$  contents drives sedimentary  $\delta^{98}\text{Mo}$  lighter than the value of overlying waters because these intermediates have  $\delta^{98}\text{Mo}$  that are lighter than the seawater value (Tossel 2005). Ancient bottom-water  $\text{H}_2\text{S}$  contents cannot be quantified using the Fe speciation proxy, nor can  $\text{H}_2\text{S}$  stability. Therefore, by analogy with modern settings,  $\delta^{98}\text{Mo}$  in some of our shale samples from the Jeerinah Formation may be isotopically lighter than the ancient seawater  $\delta^{98}\text{Mo}$  despite Fe speciation ratios indicating euxinic deposition. It is also worth noting, however, that capture of seawater  $\delta^{98}\text{Mo}$  by some sediments deposited under weakly or unstable euxinic conditions was nonetheless still plausible in an Archean ocean with low Mo availability (an idea expanded upon in the **Section 5.2.2.**).

Some geochemical trends in shales from the Klein Naute Formation may also suggest that seawater  $\delta^{98}\text{Mo}$  was not transferred to these shales. For example, Mo abundances in shales from the Klein Naute Formation are the highest of any shale unit we studied (up to 22  $\mu\text{g/g}$ ; Kendall et al. 2010). In at least some modern marine settings where sedimentary Mo abundances are very high (e.g., reaching 200  $\mu\text{g/g}$  in sediments from the Cariaco Basin [Lyons et al. 2003]), transfer of the seawater  $\delta^{98}\text{Mo}$  to sediments does not occur (Arnold et al. 2004). Sedimentary Mo abundances are extremely high in these settings today because they maintain a strong connection with the Mo-replete open ocean—a connection that provides a continuous supply of Mo (Algeo and Lyons 2006). This continuous supply of Mo, however, also hinders quantitative transfer of Mo from bottom waters to sediments in these settings. Consequently, sedimentary  $\delta^{98}\text{Mo}$  in sediments from these settings are always isotopically lighter than seawater  $\delta^{98}\text{Mo}$  (for example, because of the formation and persistence of intermediate thiomolybdates [Nägler et al. 2011]). By analogy, shales from the Klein Naute Formation that were deposited beneath a euxinic water column and have comparatively elevated Mo abundances may also possess  $\delta^{98}\text{Mo}$  that are isotopically lighter than contemporaneous seawater if they were deposited in a setting that received a steady and appreciable supply of Mo from the open ocean.

### **5.2.2. Shales deposited under locally non-euxinic conditions**

Shales we studied that were deposited beneath a non-euxinic water column are less likely to have captured the seawater  $\delta^{98}\text{Mo}$  value. The overwhelming majority of our shale samples analyzed for Mo isotopes from the Wittenoom, Mt. Sylvia, and Nauga Formations possess  $\text{Fe}_{\text{HR}}/\text{Fe}_{\text{T}}$  and  $\text{Fe}_{\text{Py}}/\text{Fe}_{\text{HR}}$  ratios indicative of non-euxinic depositional conditions (that is,  $\text{Fe}_{\text{HR}}/\text{Fe}_{\text{T}} < 0.38$  and/or  $\text{Fe}_{\text{Py}}/\text{Fe}_{\text{HR}} < 0.80$  [Poulton and Canfield 2011]). Although not as prevalent, similar Fe speciation data are also found in many of our shale samples analyzed for Mo isotopes from the Jeerinah and Klein Naute Formations.

Before continuing, it is worth noting here that the formation of pyrrhotite in ancient sedimentary rocks can lead to the misidentification of ferruginous local redox conditions (Slotznick et al. 2018). Pyrrhotite is HCl-soluble and would thus be dissolved during the  $\text{Fe}_{\text{carb}}$  extraction, in turn driving  $\text{Fe}_{\text{HR}}/\text{Fe}_{\text{T}}$  and  $\text{Fe}_{\text{Py}}/\text{Fe}_{\text{HR}}$  ratios higher and lower, respectively (towards the ranges for ferruginous ratios:  $\text{Fe}_{\text{HR}}/\text{Fe}_{\text{T}} \geq 0.38$  and  $\text{Fe}_{\text{Py}}/\text{Fe}_{\text{HR}} < 0.8$  [Poulton and Canfield 2011]). Because we did not use mineralogical, petrographic, or geochemical techniques to identify shales from our sample set that contained pyrrhotite, it is therefore theoretically possible that some of our shales with Fe speciation ratios indicative of ferruginous depositional conditions were actually deposited in an oxic or euxinic setting. Importantly, to help differentiate oxic from ferruginous local redox conditions in this subsection, we rely not only on Fe speciation data but also on accompanying trace metal data. Similarly, to account for the possibility of locally euxinic conditions during deposition of our “ferruginous” (at least according to Fe speciation data) shales, we do not rule out the idea of these shale samples capturing past seawater  $\delta^{98}\text{Mo}$  (as can happen in euxinic settings; discussed at length in the previous subsection).

Today, incomplete transfer of Mo from marine bottom-waters to sediments in non-euxinic marine settings results in sedimentary  $\delta^{98}\text{Mo}$  that are highly variable but always isotopically lighter than coeval seawater ( $\Delta^{98}\text{Mo}_{\text{seawater-sediments}} = 0 - 3\text{‰}$ ; summarized in Kendall et al. [2017]). This high degree of variability stems from the many processes shown to promote retention of lighter-mass Mo isotopes in marine sediments. For example, various combinations of complexation of Mo with Fe oxide minerals (Goldberg et al. 2009), Mn oxide minerals (Wasylenki et al. 2008), organic matter (King et al. 2018), and the formation of intermediate thiomolybdate species in sediment pore fluids and the water column (Neubert et al. 2008) can result in varying magnitudes of sedimentary enrichment in lighter-mass Mo isotopes in these settings. By analogy, the majority of our measured  $\delta^{98}\text{Mo}$  from late-Archean shales with  $\text{Fe}_{\text{HR}}/\text{Fe}_{\text{T}}$  values of  $< 0.38$  and/or  $\text{Fe}_{\text{Py}}/\text{Fe}_{\text{HR}}$  ratios of  $< 0.80$  may be isotopically lighter than contemporaneous seawater. It is difficult to estimate precisely how much lower than contemporaneous seawater  $\delta^{98}\text{Mo}$  our measured  $\delta^{98}\text{Mo}$  values are.

Shales from the Nauga Formation in GKP01 and GKF01 would be expected to have especially light  $\delta^{98}\text{Mo}$  because these samples are thought to have been deposited in an environment where  $\text{O}_2$  penetrated into marine sediments (Kendall et al. 2010). In modern marine settings where  $\text{O}_2$  penetrates into sediment pore waters, in-situ formation of Fe and Mn oxide minerals results in sedimentary  $\delta^{98}\text{Mo}$  considerably lighter than the contemporaneous seawater signature ( $\Delta^{98}\text{Mo}_{\text{seawater-sediments}} = 0.3$  to  $2.8\text{‰}$  when Fe oxides are present and  $\Delta^{98}\text{Mo}_{\text{seawater-sediments}} = 1.9$  to  $3.3\text{‰}$  when Mn oxides are present [Goldberg et al. 2012]). In support of this hypothesis, shales from the Nauga Formation have the lightest  $\delta^{98}\text{Mo}_{\text{authigenic}}$  of all the Archean shale units we studied (average  $\delta^{98}\text{Mo}_{\text{authigenic}} = 0.33\text{‰}$ ).

Shales from the Wittenoom and Mt. Sylvia Formations were most likely deposited in a locally anoxic marine environment—that is, not under the same oxidizing conditions inferred for shales from the Nauga Formation. In modern marine settings where  $O_2$  penetrates mildly into marine sediments (i.e., up to ~1 cm), Re is shown to accumulate more efficiently than does Mo (Morford et al. 2005). This geochemical pattern was found in shales from the Nauga Formation (N2 and N3) and was interpreted as evidence for mild water-column oxygenation and  $O_2$  penetration into the original marine sediments (Kendall et al. 2010). Shales from the Wittenoom and Mt. Sylvia formations, however, are not enriched in Re relative to Mo (Fig. 8). One possible interpretation of these muted Re enrichments is that the original deposition environment was well-oxygenated, thereby permitting the penetration of  $O_2$  into marine sediments to depths greater than 1 cm (conditions today that are not conducive to sedimentary Re retention [Morford et al. 2005]). However,  $\delta^{98}\text{Mo}$  in shales from the Wittenoom and Mt. Sylvia Formations (average  $\delta^{98}\text{Mo}_{\text{authigenic}} = 1.01\text{‰}$ ) are considerably heavier than those from the roughly coeval Nauga Formation (average  $\delta^{98}\text{Mo}_{\text{authigenic}} = 0.33\text{‰}$ ). Thus, these shales were probably deposited in an anoxic environment less affected by lighter-mass Mo delivery by Fe and/or Mn oxide minerals.

Just because Fe speciation ratios in these shales suggest that deposition occurred under non-euxinic conditions does not mean there was no transfer of seawater Mo and even  $\delta^{98}\text{Mo}$  to the sediments. As an example, some sediments deposited today in open-ocean continental margin settings contain  $H_2S$  strictly in shallow pore fluids but are nonetheless still fairly efficient at removing Mo from overlying waters (e.g., sediments from the Peru Margin [Poulson Brucker et al. 2009, Scholz et al. 2017]). Today, in the Mo-replete ocean, quantitative transfer of Mo is not achieved in these settings and results in a systematic isotopic offset between these sediments and seawater ( $\Delta^{98}\text{Mo}_{\text{seawater-sediments}} = \sim 0.7\text{‰}$ , an effect governed by the formation and persistence of intermediate thiomolybdate species [Siebert et al. 2006, Poulson et al. 2006, Poulson-Brucker et al. 2009, Nägler et al. 2011]). During the Archean, however, when dissolved Mo is thought to have been much less abundant in seawater than it is today (by at least an order of magnitude [Scott et al. 2008]), the Mo removal efficiency of these settings may have been sufficient enough in some instances to promote quantitative transfer to sediments. If correct, seawater  $\delta^{98}\text{Mo}$  would have been transferred to sediments in these settings. Most importantly, it would be extremely difficult to identify such settings using Fe speciation data because sedimentary Fe speciation ratios are highly variable in modern marine settings where  $H_2S$  is restricted to sediment pore fluids ( $Fe_{HR}/Fe_T$ , in particular; see Hardisty et al. [2018]).

Shales with relatively heavy  $\delta^{98}\text{Mo}$ , even if Fe speciation data suggests deposition was non-euxinic, are especially difficult to explain if the isotope data are not representative of seawater (or nearly so). For instance, two of our heaviest  $\delta^{98}\text{Mo}_{\text{authigenic}}$  come from shales of the Mt. Sylvia Formation ( $\delta^{98}\text{Mo}_{\text{authigenic}} = 1.44\text{‰}$  at 218.91m and  $2.00\text{‰}$  at 197.00m core depth). If these ancient shales did not

capture the coeval seawater  $\delta^{98}\text{Mo}$ , then it implies that seawater at that time possessed an even heavier  $\delta^{98}\text{Mo}$  (because all sediments today either capture the seawater  $\delta^{98}\text{Mo}$  value or an isotopically lighter value; summarized in Kendall et al. [2017]). Although an even heavier seawater  $\delta^{98}\text{Mo}$  cannot be ruled-out, it is worth considering that the heavier of these  $\delta^{98}\text{Mo}_{\text{authigenic}}$  already exceeds the heaviest Archean seawater  $\delta^{98}\text{Mo}$  estimates made to date (up to  $\delta^{98}\text{Mo} = \sim 1.8\text{‰}$  [Duan et al. 2010, Cabral et al. 2013]). Alternatively, these shales from the Mt. Sylvia Formation may have captured the seawater  $\delta^{98}\text{Mo}$  value.

### 5.3. Evolution of the seawater $\delta^{98}\text{Mo}$ between ~2.69 Ga and 2.50 Ga

Before we attempt to constrain the  $\delta^{98}\text{Mo}$  of late Archean seawater, it is important to first discuss some key characteristics of this signature. Namely, would our seawater  $\delta^{98}\text{Mo}$  estimates be indicative of a local or global signature, and how variable was the  $\delta^{98}\text{Mo}$  signature?

It is possible that our seawater  $\delta^{98}\text{Mo}$  estimates are representative of a well-mixed and globally homogenous open-ocean value. The paleo-basin where sedimentary rocks from the Pilbara and Kaapvaal Cratons were originally deposited is thought to have had significant water exchange with the open-ocean (Morris and Horwitz 1983, Beukes 1987, de Kock et al. 2009). Therefore, shales from both cratons were likely in contact with open-ocean seawater during original deposition. If these shales captured the coeval seawater  $\delta^{98}\text{Mo}$  value, then it was likely an open-ocean value. Moreover, previous calculations show that, even under the projected low dissolved seawater Mo abundances in the Archean ( $< 5\text{nM}$ ; Scott et al. 2008), the residence time of Mo ( $\tau_{\text{Mo}}$ ) in Archean oceans would have still been much longer than the ocean mixing time ( $\sim 1.5$  kyr today). Kendall et al. (2011) estimated an Archean  $\tau_{\text{Mo}}$  of 35 kyr assuming a modern ocean Mo input flux. A model of the Proterozoic ocean estimated a comparable  $\tau_{\text{Mo}}$  of  $> 30$  kyr (with some more unlikely scenarios still yielding  $\tau_{\text{Mo}}$  estimates  $> 3$  kyr; Dahl et al. [2011]).

Our seawater  $\delta^{98}\text{Mo}$  estimates are likely, at the minimum, to be representative of a regionally homogenous value. We argue this because we base our seawater  $\delta^{98}\text{Mo}$  estimates on Mo isotope data from sedimentary rocks from both the Pilbara and Kaapvaal Cratons (discussed in the remainder of the Section). Sedimentary rocks from these two locations are thought to have been deposited  $\sim 1,000$  km apart (de Kock et al. 2009), so any agreement in seawater  $\delta^{98}\text{Mo}$  estimates using rocks from these two locations likely signifies an at least regional seawater signature. A regional (localized) seawater  $\delta^{98}\text{Mo}$  during the Neoproterozoic is theoretically possible if the residence time of Mo in the ocean was lower than that of the ocean mixing time, despite suggestions otherwise (outlined in the previous paragraph). For example, if the size of the Archean seawater Mo reservoir has been overestimated and/or if the ocean mixing time during the Archean was longer than it is today (for example, because of limited upwelling on a faster rotating early-Earth; Olson et al. accepted), then seawater  $\delta^{98}\text{Mo}$  in an ancient basin may have been different from the  $\delta^{98}\text{Mo}$  of open-ocean seawater. One implication of a regional seawater  $\delta^{98}\text{Mo}$  is that it

may have been particularly sensitive to changes in the  $\delta^{98}\text{Mo}$  of local riverine inputs. This is because individual rivers can have highly variable, non-crustal  $\delta^{98}\text{Mo}$  (Archer and Vance 2008), even though the overwhelming majority of Mo delivered to the global ocean by rivers today is isotopically unfractionated relative to bulk upper continental crust (King and Pett-Ridge 2018).

Finally, at various times in Earth's history the seawater  $\delta^{98}\text{Mo}$  signature may have fluctuated on relatively short timescales in response to changes in ocean oxygenation (over hundreds of thousands of years during Mesozoic Oceanic Anoxic Events [e.g., Dickson 2017] to a few million years during Ediacaran Oceanic Oxygenation Events [Ostrander et al. 2019b]). Such fluctuations were possible during deposition of our shale samples and would be difficult to identify—that is, to distinguish from local controls on the  $\delta^{98}\text{Mo}$  of local sediments. Hence, we do not focus on identifying possible, relatively short-term events.

### 5.3.1. Seawater $\delta^{98}\text{Mo}$ between ~2.69 Ga and 2.63 Ga

During deposition of the Jeerinah Formation, seawater  $\delta^{98}\text{Mo}$  reached a value at least as heavy as 1.29‰ (see Figure 9). This estimate comes from the heaviest authigenic-corrected shale  $\delta^{98}\text{Mo}$  during euxinic deposition (at 68.22m core depth in AIDP3). Again, as stated earlier (**Section 5.2.1.**), there is reason to think that shales from the Jeerinah Formation may not have captured the seawater  $\delta^{98}\text{Mo}$  value. In general support of this idea, carbonates from the broadly time-equivalent Lokammona and Monteville formations (Beukes and Gutzmer 2008) in GKF01 and GKP01 may have at times also captured seawater  $\delta^{98}\text{Mo}$  and reveal slightly heavier  $\delta^{98}\text{Mo}$ : bulk-rock  $\delta^{98}\text{Mo}_{\text{NIST}+0.25\text{‰}}$  up to  $1.58 \pm 0.07\text{‰}$ ; 2SE in GKF01 and authigenic  $\delta^{98}\text{Mo}_{\text{NIST}+0.25\text{‰}}$  up to 1.95‰ in GKP01.

### 5.3.2. Seawater $\delta^{98}\text{Mo}$ between ~2.60 and 2.51 Ga

During deposition of the Wittenoom and Nauga Formations, seawater  $\delta^{98}\text{Mo}$  seems to have commonly exceeded ~1.0‰ (see Figure 9). Shales from the Wittenoom Formation are not strong candidates to have captured seawater  $\delta^{98}\text{Mo}$  (**Section 5.2.2.**). Nonetheless, calculated authigenic  $\delta^{98}\text{Mo}$  sometimes exceed 1.0‰ in these shales (9/21 samples) with the likelihood of an even heavier seawater  $\delta^{98}\text{Mo}$  during their deposition. Authigenic  $\delta^{98}\text{Mo}$  from the Nauga Formation never exceed this value, reaching only 0.61‰, but this is not surprising because shales from the Nauga Formation were likely deposited in oxic settings known in modern oceans to possess a strong preference for lighter-mass Mo isotopes (e.g., Poulson Brucker et al. 2009, Goldberg et al. 2012). Previously reported  $\delta^{98}\text{Mo}$  in time-equivalent bulk-shale and carbonate samples from the Campbellrand-Malmani carbonate platform also sometimes exceed 1.0‰, peaking at values as high as  $1.40 \pm 0.11\text{‰}$ ; 2SE (Eroglu et al. 2015).

Seawater  $\delta^{98}\text{Mo}$  may have been especially heavy during deposition of the Mt. Sylvania and uppermost Nauga formations. One of our shale samples from the Mt. Sylvania Formation has an extremely heavy calculated authigenic  $\delta^{98}\text{Mo}$  value of 2.00‰ (at 197m core depth in ABDP9). An exceptionally heavy bulk-rock  $\delta^{98}\text{Mo}$  of  $1.70 \pm 0.02\%$ ; 2SE was also found previously in a shale sample from the uppermost Nauga Formation in GKP01 (Wille et al. 2007).

### 5.3.3. Seawater $\delta^{98}\text{Mo}$ at 2.50 Ga

During deposition of the Klein Naute Formation, seawater  $\delta^{98}\text{Mo}$  reached a composition of at least 1.59‰ (see Figure 9). This value is equal to the heaviest of our authigenic-corrected  $\delta^{98}\text{Mo}$  for a shale in the Klein Naute Formation (at 274.23m core depth in GKF01). These shales are plausible candidates for having at times captured and preserved seawater  $\delta^{98}\text{Mo}$  (**Section 5.2.1.**). Shales from the time-equivalent Mt. McRae Shale in Western Australia that were also deposited under euxinic conditions (Reinhard et al. 2009), and therefore possibly captured seawater  $\delta^{98}\text{Mo}$ , possess a similar maximum authigenic-corrected  $\delta^{98}\text{Mo}$  (1.64‰ [Ostrander et al. 2019a]), as do bulk rock  $\delta^{98}\text{Mo}$  from carbonates in the Klein Naute Formation ( $\delta^{98}\text{Mo}_{\text{NIST}+0.25\%} = 1.53 \pm 0.02\%$ ; 2SE, also in GKF01 [Voegelin et al. 2010]). This agreement, despite differences in geographic location (South Africa versus Western Australia) and lithology (carbonates versus shales), bolsters support for our 2.50 Ga seawater  $\delta^{98}\text{Mo}$  signature estimate.

### 5.4. Marine oxygenation during the runup to the GOE

It is now evident from our updated shale dataset that seawater  $\delta^{98}\text{Mo}$  between ~2.69 Ga and 2.50 Ga was commonly greater than 1.0‰ (and also apparent in Fig. 9), much more so than was previously recognized. In Wille et al. (2007),  $\delta^{98}\text{Mo}$  in shales from South Africa greater than 1.0‰ were found exclusively in the uppermost Lower Nauga Formation and its overlying strata. In Voegelin et al. (2010), authigenic  $\delta^{98}\text{Mo}$  exceeding 1.0‰ were found sporadically throughout the GKP01 drill core (in the Boomplaas and Monteville Formations, the Upper and Lower Nauga Formations, and the Klein Naute Formation). Molybdenum isotope compositions also sporadically exceed 1.0‰ in the coeval but more proximal carbonates and shales from the Campbellrand-Malmani carbonate platform (Eroglu et al. 2015). In studies of rocks from Western Australia,  $\delta^{98}\text{Mo}$  greater than 1.0‰ were found previously in one iron formation sample from the Marra Mamba Formation, one shale sample from the Mt. Sylvania Formation, and many samples from the Mt. McRae Shale (Kurzweil et al. 2015, Duan et al. 2010, Ostrander et al. 2019a). In most cases, and beyond the lower sample resolution of these earlier studies, the relative lack of heavy sedimentary  $\delta^{98}\text{Mo}$  values was probably a consequence of detrital dilution and local redox conditions, effects that also skewed some of our shale  $\delta^{98}\text{Mo}$  to isotopically lighter values (see **Section 5.1.** and **Section 5.2.**).



Such heavy seawater  $\delta^{98}\text{Mo}$  values during the late-Archean require a marine sink for Mo with a strong preference for lighter-mass isotopes (assuming no measurable Mo isotope fractionation is expressed during delivery of Mo to the ocean; see King and Pett-Ridge [2018]). Today, there are some anaerobic processes shown to promote the preferential retention of lighter-mass Mo isotopes in marine sediments. Organic matter (OM), for example, can preferentially retain lighter-mass isotopes during Mo adsorption ( $\Delta^{98}\text{Mo}_{\text{solution-OM}} = 0.63\text{‰} - 1.79\text{‰}$  [King et al. 2018]) and could have been produced during anoxygenic photosynthesis in shallow waters of the late-Archean ocean (for example, by photoferrotrophs [Konhauser et al. 2002]). Also, the presence of intermediate thiomolybdate species in marine bottom waters or sediments is shown to promote the retention of lighter-mass Mo isotopes in sediments (up to  $\Delta^{98}\text{Mo}_{\text{solution-sediment}} = \sim 3.0\text{‰}$  [Neubert et al. 2008]) and require only a low or unstable local  $\text{H}_2\text{S}$  inventory (Helz et al. 1996, Erickson and Helz 2000). Lastly, Fe oxide minerals preferentially remove lighter-mass Mo isotopes from seawater ( $\Delta^{98}\text{Mo}_{\text{solution-oxide}} = 0.83\text{‰} - 2.19\text{‰}$  [Goldberg et al. 2009]). They possess multiple anaerobic formation pathways (photo-oxidation [Cairns-Smith 1978] and photoferrotrophy [Widdel et al. 1993]) fully independent of  $\text{O}_2$  availability, and they readily formed in late-Archean marine settings (Konhauser et al. 2017).

All or some of the anaerobic processes noted above probably operated during the late-Archean and were thus at least partly responsible for driving the heavy seawater  $\delta^{98}\text{Mo}$  inferred here. Unfortunately, it is impossible using only the Mo isotope paleoredox proxy to differentiate the effects of these anaerobic Mo isotope fractionation pathways from those that would have required  $\text{O}_2$ . For example, Fe oxides are also formed in the presence of  $\text{O}_2$ , and it is currently impossible using Mo isotopes to differentiate this formation pathway from an anaerobic one. Furthermore, although Mn oxide mineral formation is more intimately linked to  $\text{O}_2$  (e.g., Calvert and Pedersen 1996), the observed isotope fractionation effect imparted during adsorption of Mo to Mn oxides ( $\Delta^{98}\text{Mo}_{\text{solution-oxide}} = 2.7 \pm 0.1\text{‰}$  [Wasylenki et al. 2008]) is very similar to that observed during the formation and persistence of intermediates among the thiomolybdate complexes under weakly euxinic conditions (up to  $\Delta^{98}\text{Mo}_{\text{solution-sediment}} = \sim 3.0\text{‰}$  in shallower-water sediments situated not far below the chemocline in the Black Sea [Neubert et al. 2008]). These overlaps make identification of ancient Mo isotope fractionation pathways nearly impossible.

Despite the many alternatives, it is plausible, if not likely, that Fe and Mn oxide minerals formed in  $\text{O}_2$ -bearing waters of late-Archean oceans were at least partly responsible for a heavy seawater  $\delta^{98}\text{Mo}$ . Many independent lines of geochemical evidence, some from the same sedimentary rocks targeted in our study, suggest that  $\text{O}_2$ -bearing waters were fairly common in at least local portions of the shallow ocean within the Hamersley and Griqualand West basins during the final two-hundred million years of the Archean (described below).



#### 5.4.1. Marine oxygenation between ~2.69 Ga and 2.63 Ga

Geochemical trends found in organic-rich shales from the Jeerinah Formation suggest that  $O_2$  was produced and accumulated at least transiently in Earth's ocean during its deposition. In Scott et al. (2011), a case was made based on Fe speciation data that the high abundance of TOC in shales from the Jeerinah Formation was not a product of anoxygenic photosynthesis in the ancient overlying water column. Thus, by elimination, oxygenic photosynthesis was the most likely culprit for driving these high sedimentary TOC abundances (also see Lyons et al. 2014). Heavy nitrogen (N) isotope compositions found in shales from the Jeerinah Formation support this suggestion because they are thought to require the operation of an aerobic N cycle in oxygenated shallow waters (Koehler et al. 2018).

Evidence for ancient ocean oxygenation is also present in stratum coeval to the Jeerinah Formation. Low Fe speciation ratios indicative of local oxic depositional conditions (i.e.,  $Fe_{HR}/Fe_T < 0.22$  and  $Fe_{PY}/Fe_{HR} < 0.70$  [Poulton and Canfield 2011]) are found in some shale samples from the Lokamonna and Monteville formations from South Africa (Zerkle et al. 2012). As in the Jeerinah Formation, heavy N isotope compositions that require a local aerobic N cycle are also found in the Monteville Formation (Godfrey and Falkowski 2009). Lastly, a surface-to-deep carbon (C) isotope gradient inferred from bulk rock and kerogen in shallow-water carbonates from South Africa, Zimbabwe, Canada, and Western Australia (including in the Jeerinah Formation) is interpreted as evidence for the accumulation of  $O_2$  in shallow waters above large areas of global continental margins after about 2.7 Ga (Eigenbrode and Freeman 2006).

#### 5.4.2. Marine oxygenation between ~2.60 Ga and 2.51 Ga

Geochemical trends in the Nauga Formation from South Africa also point to at least transient marine oxygenation during their deposition. In discrete shale beds from the Nauga Formation, elevated rhenium (Re) abundances are accompanied by near-crustal Mo abundances (Kendall et al. 2010). This geochemical fingerprint is found today in marine sediments when  $O_2$  is present in local marine bottom waters and also penetrates into sediment pore fluids (up to 1 cm below the sediment-water interface [Morford et al. 2005]). Heavy N isotope compositions requiring oxygenated surface waters are also found in kerogen from sedimentary rocks in the Nauga Formation (Godfrey and Falkowski 2009).

#### 5.4.3. Marine oxygenation at 2.50 Ga

Late-Archean marine oxygenation seems to have reached an apex at 2.50 Ga, evident by the many geochemical trends found in sedimentary rocks from this age that suggest a “whiff” of atmospheric and marine  $O_2$  occurred at that time (Anbar et al. 2007, Kaufman et al. 2007, Garvin et al. 2009, Reinhard

et al. 2009, Duan et al. 2010, Kendall et al. 2013, 2015, Stüeken et al. 2015, Gregory et al. 2015, Ostrander et al. 2019a). In Kaufman et al. (2007), the case was made for an oxidative marine S cycle at 2.50 Ga on the basis of large magnitudes of negative MDF-S preserved in the upper member of the Mt. McRae Shale from Western Australia and one of its South African equivalents (the Gamohaian Formation). Heavy N isotope compositions are also found in the upper member of the Mt. McRae Shale, suggesting the presence of O<sub>2</sub> in ancient shallow waters (Garvin et al. 2009). Positive selenium (Se; Stüeken et al. [2015]), Mo (Duan et al. 2010), and uranium (U; Kendall et al. [2013]) isotope compositions found in the upper Mt. McRae Shale may also fingerprint the presence of marine O<sub>2</sub> at 2.50 Ga. Finally, an anti-correlation between Mo and thallium (Tl) isotopes in the upper Mt. McRae Shale suggests that Mn oxide burial in oxygenated marine sediments beneath fully oxygenated water columns at 2.50 Ga was widespread on at least a regional scale (Ostrander et al. 2019a). For such widespread Mn oxide burial to have occurred, dissolved O<sub>2</sub> may have accumulated at depth over a potentially large area of global continental margins.

A noticeable  $\delta^{98}\text{Mo}$  increase is still present within the sedimentary record at around 2.50 Ga and corroborates the “whiff” hypothesis (Fig. 9; and also see Wille et al. [2007] and Kurzweil et al. [2015]). In light of our updated dataset, however, it is worth noting the comparable increase in sedimentary  $\delta^{98}\text{Mo}$  found in a few shale samples deposited just before 2.50 Ga— in the Mt. Sylvia Formation (this study) and the uppermost Nagua Formation (Wille et al. 2007) (see Fig. 9). At face value, these heavier  $\delta^{98}\text{Mo}$  could suggest that Earth’s pre-GOE oceans became more well-oxygenated (at least transiently) earlier than was previously recognized. This suggestion may gain merit from the kerogen N isotope record because it shows suggestions of a coeval shift to positive values within the uppermost Nauga Formation that are not seen in similar magnitude within older strata (Godfrey and Falkowski 2009). Further investigation is needed to test this hypothesis.

## 6. Conclusions

We presented new  $\delta^{98}\text{Mo}$  data from 140 shale samples deposited between ~2.69 Ga and 2.50 Ga, on the eve of the GOE. Critically, and unlike most previous investigations, the local redox conditions during deposition of our shales were independently constrained using the Fe speciation proxy. These depositional redox constraints are extremely important because transfer of the seawater  $\delta^{98}\text{Mo}$  to sediments is shown today to be linked to local redox. Our new dataset therefore provides us with a unique opportunity to estimate the evolution of seawater  $\delta^{98}\text{Mo}$  during the final two hundred million years of the Archean Eon.

As is the case today, most of the shales we targeted that were deposited under non-euxinic conditions are unlikely to have captured and preserved contemporaneous seawater  $\delta^{98}\text{Mo}$ . Instead,  $\delta^{98}\text{Mo}$

preserved in these shales are probably skewed toward values lighter than those of ancient seawater. Today, lighter-mass Mo isotopes preferentially accumulate in non-euxinic marine sediments during complexation with Fe and Mn oxide minerals, organic matter, and in the presence of intermediate thio-complexes. Some combination of these processes probably also governed the  $\delta^{98}\text{Mo}$  of our ancient shales deposited under analogous conditions.

Also akin to today, some of the shales we targeted that were deposited under euxinic conditions may have captured seawater  $\delta^{98}\text{Mo}$ . Guided by the  $\delta^{98}\text{Mo}$  data primarily from these shales, we infer a late-Archean seawater  $\delta^{98}\text{Mo}$  that commonly exceeded 1.0‰. Such a heavy seawater  $\delta^{98}\text{Mo}$  could be explained by the preferential retention of lighter-mass Mo isotopes in marine sediments during strictly anaerobic processes in the late-Archean ocean (e.g., during the formation of organic matter, phototrophic Fe oxides, or intermediate thio-complexes). It is also highly plausible, however, that lighter-mass Mo isotopes were preferentially retained by Fe and Mn oxide minerals formed in oxygenated shallow waters of the pre-GOE ocean. In fact, many independent lines of geochemical evidence suggest that Earth's shallow oceans were commonly oxygenated during the final two-hundred million years of the Archean Eon, lending support to this idea.

One strategy moving forward would be to pair the Mo isotope palaeoredox proxy with other proxies to better differentiate anaerobic from aerobic processes. Thallium isotopes may prove useful because the Tl isotope composition of seawater is also thought to be set in-part by global ocean oxygenation and was shown recently to be transferred to sediments in modern euxinic marine settings (Owens et al. 2017). Accordingly, the same shale sample sets targeted here for Mo isotopes could also be targeted for complementary Tl isotope analyses. An additional benefit of pairing together Tl and Mo isotopes is that, unlike Mo, Tl isotopes would not be expected to fractionate during the anaerobic processes that complicate Mo isotope interpretations (e.g., during adsorption to Fe oxides or during formation of thio-complex intermediates [discussed in Ostrander et al. 2019a]). The uranium (U) isotope palaeoredox proxy may also be useful because the U isotope composition of seawater is shown to be set in part by ocean oxygenation and can be inferred from carbonates (which typically have minor isotopic offset from the seawater value [Romaniello et al. 2013, Tissot et al. 2018]). Measuring U isotope ratios in carbonates deposited between ~2.7 Ga and 2.5 Ga would be a useful way to cross check the sometimes heavy  $\delta^{98}\text{Mo}$  found in the late-Archean carbonate record (which may also have at times captured seawater  $\delta^{98}\text{Mo}$  [Voegelin et al. 2010]). If shallow ocean oxygenation was indeed recurrent during the Neoproterozoic, as we posit here based on an expanded shale  $\delta^{98}\text{Mo}$  record, then this oxygenation should also be fingerprinted in the contemporaneous sedimentary Tl and U isotope records.

## References

- Algeo T.J., Lyons, T.W., 2006. Mo-total organic carbon covariation in modern anoxic marine environments: Implications for analysis of paleoredox and paleohydrographic conditions. *Paleoceanography* 21, PA1016 1-23.
- Altermann, W., Nelson, D.R., 1998. Sedimentation rates, basin analysis and regional correlation of three Neoproterozoic and Paleoproterozoic sub-basins of the Kaapvaal craton as implied by precise SHRIMP U-Pb zircon ages from volcanic sediments. *Journal of Sedimentary Geology* 120, 225-256.
- Anbar, A.D., Duan, Y., Lyons, T.W., Arnold, G.L., Kendall, B., Creaser, R.A., Kaufman, A.J., Gordon, G.W., Scott, C., Garvin, J., Buick, R., 2007. A whiff of oxygen before the great oxidation event? *Science* 317, 1903-1906.
- Archer, C., Vance, D., 2008. The isotopic signature of the global riverine molybdenum flux and anoxia in the ancient oceans. *Nature Geoscience* 1, 597-600.
- Arndt, N.T., Nelson, D.R., Compston, W., Trendall, A.F., Thorne, A.M., 1991. The age of the Fortesque Group, Hamersley basin, Western Australia, from ion microprobe U-Pb zircon results. *Australian Journal of Earth Sciences* 38, 261-281.
- Arnold, G.L., Anbar, A.D., Barling, J., Lyons, T.W., 2004. Molybdenum isotope evidence for widespread anoxia in Mid-Proterozoic oceans. *Science* 304, 87-90.
- Barling, J., Arnold, G.L., Anbar, A.D., 2001. Natural mass-dependent variations in the isotopic composition of molybdenum. *Earth and Planetary Science Letters* 193, 447-457.
- Bekker, A., Holland, H.D., Wang, P-L., Rumble III, D., Stein, H.J., Hannah, J.L., Coetzee, L.L., Beukes, N.J., 2004. Dating the rise of atmospheric oxygen. *Nature* 427, 117-120.
- Beukes, N.J., 1987. Facies relations, depositional environments and diagenesis in a major early Proterozoic stromatolitic carbonate platform to basinal sequence, Campbellrand Subgroup, Transvaal Supergroup, Southern Africa. *Sedimentary Geology* 54, 1-46.
- Beukes, N.J., Gutzmer, J., 2008. Origin and Paleoenvironmental Significance of Major Iron Formations at the Archean-Paleoproterozoic Boundary. *Society of Economic Geologists Reviews* 15, 5-47.
- Brocks, J.J., Buick, R., Logan, G.A., Summons, R.E., 2003. Composition and syngeneity of molecular fossils from the 2.78 to 2.45 billion-year-old Mount Bruce Supergroup, Pilbara Craton, Western Australia. *Geochimica et Cosmochimica Acta* 67, 4289-4319.
- Bura-Nakić, E., Andersen, M.B., Archer, C., de Souza, G.F., Marguš, M., Vance, D., 2018. Coupled Mo-U abundances and isotopes in a small marine euxinic basin: Constraints on processes in euxinic basins. *Geochimica et Cosmochimica Acta* 222, 212-229.
- Cabral, A. R., Creaser, R. A., Nägler, T., Lehmann, B., Voegelin A. R., Belyatsky, B., Pašava, J., Seabra Gomes Jr., A. A., Galbiatti, H., Böttcher, M. E., Escher, P., 2013. Trace element and multi-

- isotope geochemistry of Late-Archean black shales in the Carajás iron-ore district, Brazil. *Chemical Geology* 362, 91-104.
- Cairns-Smith, A.G., 1978. Precambrian solution photochemistry, inverse segregation, and banded iron formation. *Nature* 276, 807-808.
- Calvert, S. E., Pedersen, T. F., 1996. Sedimentary geochemistry of manganese: implications for the environment of formation of manganiferous black shales. *Economic Geology* 91, 36-47.
- Chen, X., Ling, H-F, Vance, D., Shields-Zhou, G.A., Zhu, M., Poulton, S.W., Och, L.M., Jiang, S-Y, Li, D., Cremonese, L., Archer, C., 2015. Rise to modern levels of ocean oxygenation coincided with the Cambrian radiation of animals. *Nature Communications* 6, 7142.
- Chen, X., Romaniello, S.J., Herrmann, A.D., Hardisty, D., Gill, B.C., Anbar, A.D., 2018. Diagenetic effects on uranium isotope fractionation in carbonate sediments from the Bahamas. *Geochimica et Cosmochimica Acta* 237, 294-311.
- Dahl, T.W., Hammarlund, E.U., Anbar, A.D., Bond, D.P.G., Gill, B.C., Gordon, G.W., Knoll, A.H., Nielsen, A.T., Schovsbo, N.H., Canfield, D.E., 2010. Devonian rise in atmospheric oxygen correlated to the radiations of terrestrial plants and large predatory fish. *Proceedings of the National Academy of Sciences* 107, 17911–17915.
- Dahl, T.W., Canfield, D.E., Rosing, M.T., Frei, R.E., Gordon, G.W., Knoll, A.H., Anbar, A.D., 2011. Molybdenum evidence for expansive sulfidic water masses in ~750 Ma oceans. *Earth and Planetary Science Letters* 311, 264-274.
- de Kock, M.O., Evans, D.A.D., Beukes, N.J., 2009. Validating the existence of Vaalbara in the Neoproterozoic. *Precambrian Research* 174, 145-154.
- Dickson, A.J., 2017. A molybdenum-isotope perspective on Phanerozoic deoxygenation events. *Nature Geoscience* 10, 721-726.
- Duan, Y., Anbar, A.D., Arnold, G.L., Lyons, T.W., Gordon, G.W., Kendall, B., 2010. Molybdenum isotope evidence for mild environmental oxygenation before the Great Oxidation Event. *Geochimica et Cosmochimica Acta* 74, 6655-6668.
- Eigenbrode, J.L., Freeman, K.H., 2006. Late Archean rise of aerobic microbial ecosystems. *Proc. Natl. Acad. Sci.* 103, 15759-15764.
- Erickson, B.E., Helz, G.R., 2000. Molybdenum(VI) speciation in sulfidic waters: Stability and lability of thiomolybdates. *Geochimica et Cosmochimica Acta* 64, 1149-1158.
- Eroglu, S., Schoenberg, R., Wille, M., Beukes, N., Taubald, H., 2015. Geochemical stratigraphy, sedimentology, and Mo isotope systematics of the ca. 2.58-2.50 Ga-old Transvaal Supergroup carbonate platform, South Africa. *Precambrian Research* 266, 27-46.

- Farquhar, J., Bao, H., Thiemens, M., 2000. Atmospheric influence of Earth's earliest sulfur cycle. *Science* 289, 756-758.
- French, K.L., Hallmann, C., Hope, J.M., Schoon, P.L., Zumberge, J.A., Hoshino, Y., Peters, C.A., George, S.C., Love, G.D., Brocks, J.J., Buick, R., Summons, R.E., 2015. Reappraisal of hydrocarbon biomarkers in Archean rocks. *Proceedings of the National Academy of Sciences* 112, 5915-5920.
- Garvin, J., Buick, R., Anbar, A. D., Arnold, G. L., Kaufman, A. J., 2009. Isotopic evidence for an aerobic nitrogen cycle in the latest Archean. *Science* 323, 1045-1048.
- Godfrey, L.V., Falkowski, P.G., 2009. The cycling and redox state of nitrogen in the Archaean ocean. *Nature Geoscience* 2, 725-729.
- Goldberg, T., Archer, C., Vance, D., Poulton, S.W., 2009. Mo isotope fractionation during adsorption to Fe (oxyhydr) oxides. *Geochimica et Cosmochimica Acta* 73, 6502–6516.
- Goldberg, T., Archer, C., Vance, D., Thamdrup, B., McAnena, A., Poulton, S.W., 2012. Controls on Mo isotope fractionations in a Mn-rich anoxic marine sediment, Gullmar Fjord, Sweden. *Chemical Geology* 296-297, 73-82.
- Goldberg, T., Gordon, G., Izon, G., Archer, C., Pearce, C.R., McManus, J., Anbar, A.D., Rehkämper, M., 2013. Resolution of inter-laboratory discrepancies in Mo isotope data: an intercalibration. *Journal of Analytical Atomic Spectrometry* 28, 724-735.
- Greber, N.D., Pettke, T., Nägler, T.F., 2014. Magmatic-hydrothermal molybdenum isotope fractionation and its relevance to the igneous crustal signature. *Lithos* 190-191, 104-110.
- Greber, N.D., Puchtel, I.S., Nägler, T.F., Mezger, K., 2015. Komatiites constrain molybdenum isotope composition of Earth's mantle. *Earth and Planetary Science Letters* 421, 129-138.
- Gregory, D. D., Large, R. R., Halpin, J. A., Steadman, J. A., Hickman, A. H., Ireland, T. R., Holden, P., 2015. The chemical conditions of the late Archean Hamersley basin inferred from whole rock and pyrite geochemistry with  $\Delta^{33}\text{S}$  and  $\delta^{34}\text{S}$  isotope analyses. *Geochimica et Cosmochimica Acta* 149, 223-250.
- Gumsley, A.P., Chamberlain, K.R., Bleeker, W., Söderlund, U., de Kock, M.O., Larsson, E.R., Bekker, A., 2017. Timing and tempo of the Great Oxidation Event. *Proceedings of the National Academy of Sciences* 114, 1811-1816.
- Hardisty, D. S., Lyons, T. W., Riedinger, N., Isson, T. T., Owens, J. D., Aller, R. C., Rye, D. M., Planavsky, N. J., Reinhard, C. T., Gill, B. C., Masterson, A. L., Asael, D. and Johnston, D. T., 2018. An evaluation of sedimentary molybdenum and iron as proxies for pore fluid paleoredox conditions. *American Journal of Science* 318, 527-556.



- Helz, G.R., Miller, C.V., Charnock, J.M., Mosselmans, J.F.W., Pattrick, R.A.D., Garner, C.D., Vaughan, D.J., 1996. Mechanism of molybdenum removal from the sea and its concentration in black shales: EXAFS evidence. *Geochimica et Cosmochimica Acta* 60, 3631-3642.
- Kasting, J.F., 1992. Models relating to Proterozoic atmospheric and ocean chemistry. In: Schopf, J., Klein, C. (Eds), *The Proterozoic Biosphere, A Multidisciplinary Study*. Cambridge University Press, 1185-1187.
- Kaufman, A. J., Johnston, D. T., Farquhar, J., Masterson, A. L., Lyons, T. W., Bates. S., Anbar, A. D., Arnold, G. L., Garvin, J., Buick, R., 2007. Late Archean biospheric oxygenation and atmospheric evolution. *Science* 317, 1900-1903.
- Kendall, B., Reinhard, C.T., Lyons, T.W., Kaufman, A.J., Poulton, S.W., Anbar, A.D., 2010. Pervasive oxygenation along late Archaean ocean margins. *Nature Geoscience* 3, 647-652.
- Kendall, B., Gordon, G.W., Poulton, S.W., Anbar, A.D., 2011. Molybdenum isotope constraints on the extent of late Paleoproterozoic ocean euxinia. *Earth and Planetary Science Letters* 307, 450-460.
- Kendall, B., Brennecka, G. A., Weyer, S., Anbar, A. D., 2013. Uranium isotope fractionation suggests oxidative uranium mobilization at 2.50 Ga. *Chemical Geology* 362, 105-114.
- Kendall, B., Creaser, R.A., Reinhard, C.T., Lyons, T.W., Anbar, A.D., 2015. Transient episodes of mild environmental oxygenation and oxidative continental weathering during the late Archaean. *Science Advances* 1:e1500777.
- Kendall, B., Dahl, T.W., Anbar, A.D., 2017. Good golly, why Moly? The stable isotope geochemistry of molybdenum. *Reviews in Mineralogy and Geochemistry* 82, 682-732.
- King, E.K., Perakis, S.S., Pett-Ridge, J.C., 2018. Molybdenum isotope fractionation during adsorption to organic matter. *Geochimica et Cosmochimica Acta* 222, 584-598.
- King, E.K., Pett-Ridge, J.C., 2018. Reassessing the dissolved molybdenum isotopic composition of ocean inputs: The effect of chemical weathering and groundwater. *Geology* 46, 955-958.
- Koehler, M.C., Buick, R., Kipp, M.A., Stüeken, E.E., Zaloumis, J., 2018. Transient surface ocean oxygenation recorded in the ~2.66-Ga Jeerinah Formation, Australia. *Proc. Natl. Acad. Sci.* 115, 7711-7716.
- Konhauser, K.O., Hamade, T., Raiswell, R., Morris, R.C., Ferris, F.G., Southam, G., Canfield, D.E., 2002. Could bacteria have formed Precambrian banded iron formations? *Geology* 30, 1079-1082.
- Konhauser, K.O., Lalonde, S.V., Planavsky, N.J., Pecoits, E., Lyons, T.W., Mojzsis, S.J., Rouxel, O.J., Barley, M.E., Rosière, C., Fralick, P.W., Kump, L.R., Bekker, A., 2011. Aerobic bacterial pyrite oxidation and acid rock drainage during the Great Oxidation Event. *Nature* 478, 369-373.
- Konhauser, K.O., Planavsky, N.J., Hardisty, D.S., Robbins, L.J., Warchola, T.J., Hugaard, R., Lalonde, S.V., Partin, C.A., Oonk, P.B.H., Tsikos, H., Lyons, T.W., Bekker, A., Johnson, C.M., 2017. Iron



- formations: A global record of Neoproterozoic to Palaeoproterozoic environmental history. *Earth-Science Reviews* 172, 140-177.
- Kurzweil, F., Wille, M., Schoenberg, R., Taubald, H., Van Kranendonk, M.J., 2015. Continuously increasing  $\delta^{98}\text{Mo}$  values in Neoproterozoic black shales and iron formations from the Hamersley Basin. *Geochimica et Cosmochimica Acta* 164, 523-542.
- Lalonde, S.V., Konhauser, K.O., 2015. Benthic perspective on Earth's oldest evidence for oxygenic photosynthesis. *Proc. Natl. Acad. Sci.* 112, 995-1000.
- Luo, G., Ono, S., Beukes, N.J., Wang, D.T., Xie, S., Summons, R.E., 2016. Rapid oxygenation of Earth's atmosphere 2.33 billion years ago. *Science Advances* 2:e1600134.
- Lyons, T. W., Werne, J. P., Hollander, D. J., Murray, R. W., 2003. Contrasting sulfur geochemistry and Fe/Al and Mo/Al ratios across the last oxic-to-anoxic transition in the Cariaco Basin, Venezuela. *Chemical Geology* 195, 131-157.
- Lyons, T.W., Reinhard, C.T., Planavsky, N.J., 2014. The rise of oxygen in Earth's early ocean and atmosphere. *Nature* 506, 307-315.
- McCoy-West, A.J., Chowdhury, P., Burton, K.W., Sossi, P., Nowell, G.M., Fitton, J.G., Kerr, A.C., Cawood, P.A., Williams, H.M., 2019. Extensive crustal extraction in Earth's early history inferred from molybdenum isotopes. *Nature Geoscience* <https://doi.org/10.1038/s41561-019-0451-2>.
- Miyano, T., Beukes, N.J., 1984. Phase relations of stilpnomelane, ferriannite, and riebeckite in very low-grade metamorphosed iron formations. *Geological Society of South Africa Transactions* 87, 111-124.
- Morford, J.L., Emerson, S.R., Breckel, E.J., Kim, S.H., 2005. Diagenesis of oxyanions (V, U, Re, and Mo) in pore waters and sediments from a continental margin. *Geochimica et Cosmochimica Acta* 69, 5021-5032.
- Morris, R.C., Horwitz, R.C., 1983. The origin of the iron-formation-rich Hamersley group of Western Australia – deposition on a platform. *Precambrian Research* 21, 273-297.
- Nägler, T.F., Neubert, N., Böttcher, M.E., Dellwig, O., Schnetger, B., 2011. Molybdenum isotope fractionation in pelagic euxinia: evidence from the modern Black and Baltic Seas. *Chemical Geology* 289, 1-11.
- Nägler, T.F., Anbar, A.D., Archer, C., Goldberg, T., Gordon, G.W., Greber, N.D., Siebert, C., Sohrin, Y., Vance, D., 2014. Proposal for an international molybdenum isotope measurement standard and data representation. *Geostandards and Geoanalytical Research* 38, 149–151.
- Nelson, D.R., Trendall, A.F., Alterman, W., 1999. Chronological correlation between the Pilbara and Kaapvaal cratons. *Precambrian Research* 97, 165-189.

- Neubert, N., Nägler, T.F., Böttcher, M.E., 2008. Sulfidity controls molybdenum isotope fractionation into euxinic sediments: evidence from the modern Black Sea. *Geology* 36, 775-778.
- Noordmann, J., Weyer, S., Montoya-Pino, C., Dellwig, O., Neubert, N., Eckert, S., Paetzel, M., Böttcher, M.E., 2015. Uranium and molybdenum isotope systematics in modern euxinic basins: case studies from the central Baltic Sea and the Kyllaren fjord (Norway). *Chemical Geology* 396, 182-195.
- Olson, S.L., Kump, L.R., Kasting, J.F., 2013. Quantifying the areal extent and dissolved oxygen concentrations of Archean oxygen oases. *Chem. Geol.* 362, 35-43.
- Olson, S.L., Ostrander, C.M., Gregory, D.D., Roy, M., Anbar, A.D., Lyons, T.W., 2019. Volcanically modulated pyrite burial and ocean-atmosphere oxidation. *Earth and Planetary Science Letters* 506, 417-427.
- Olson, S.L., Jansen, M.F., Abbot, D.S., 2019. Oceanographic constraints on exoplanet life. arXiv: 1909.02928 [astro-ph.EP]
- Ostrander, C.M., Nielsen, S.G., Owens, J.D., Kendall, B., Gordon, G.W., Romaniello, S.J., Anbar, A.D., 2019a. Fully oxygenated water columns over continental shelves before the Great Oxidation Event. *Nature Geoscience* 12, 186-191.
- Ostrander, C.M., Sahoo, S.K., Kendall, B., Jiang, G., Planavsky, N.J., Lyons, T.W., Nielsen, S.G., Owens, J.D., Gordon, G.W., Romaniello, S.J., Anbar, A.D., 2019b. Multiple negative molybdenum isotope excursions in the Doushantuo Formation (South China) fingerprint complex redox-related processes in the Ediacaran Nanhua Basin. *Geochimica et Cosmochimica Acta* 261, 191-209.
- Owens, J.D., Nielsen, S.G., Horner, T.J., Ostrander, C.M., Peterson, L.C., 2017. Thallium-isotopic compositions of euxinic sediments as a proxy for global manganese-oxide burial. *Geochim. Cosmochim. Acta* 213, 291-307.
- Pavlov, A.A., Kasting, J.F., 2002. Mass-independent fractionation of sulfur isotopes in Archean sediments: strong evidence for an anoxic Archean atmosphere. *Astrobiology* 2, 27-41.
- Philippot, P., Ávila, J.N., Killingsworth, B.A., Tessalina, S., Baton, F., Caquineau, T., Muller, E., Pecoits, E., Cartigny, P., Lalonde, S.V., Ireland, T., Thomazo, C., Kranendonk, M.J., Busigny, V., 2018. Globally asynchronous sulphur isotope signals require re-definition of the Great Oxidation Event. *Nature Communications* 9, 2245.
- Poulson, R. L., Siebert, C., McManus, J., Berelson, W. M., 2006. Authigenic molybdenum isotope signatures in marine sediments. *Geology* 34, 617-620.

- Poulson Brucker, R.L., McManus, J., Severmann, S., Berelson, W.M., 2009. Molybdenum behavior during early diagenesis: Insights from Mo isotopes. *Geochemistry, Geophysics, Geosystems* 10, Q06010.
- Poulton, S.W., Canfield, D.E., 2011. Ferruginous conditions: A dominant feature of the ocean through Earth's history. *Elements* 7, 107-112.
- Raiswell, R., Hardisty, D.S., Lyons, T.W., Canfield, D.E., Owens, J.D., Planavsky, N.J., Poulton, S.W., Reinhard, C.T., 2018. The iron paleoredox proxies: a guide to pitfalls, problems and proper practice. *American Journal of Science* 318, 491-526.
- Reinhard, C.T., Raiswell, R., Scott, C., Anbar, A.D., Lyons, T.W., 2009. A late Archean sulfidic sea stimulated by early oxidative weathering of the continents. *Science* 326, 713-716.
- Romaniello, S. J., Herrmann, A. D., Anbar, A. D., 2013. Uranium concentrations and  $^{238}\text{U}/^{235}\text{U}$  isotope ratios in modern carbonates from the Bahamas: Assessing a novel paleoredox proxy. *Chemical Geology* 362, 305-316.
- Rudnick, R.L., Gao, S., 2003. Composition of the continental crust. In *The Crust*, vol. 3 (ed. R.L. Rudnick). Elsevier, 1-64.
- Scholz, F., Siebert, C., Dale, A.W., Frank, M., 2017. Intense molybdenum accumulation in sediments underneath a nitrogenous water column and implications for the reconstruction of paleo-redox conditions based on molybdenum isotopes. *Geochimica et Cosmochimica Acta* 213, 400-417.
- Schröder, S., Lacassie, J.P., Beukes, N.J., 2006. Stratigraphic and geochemical framework of the Agouron drill cores, Transvaal Supergroup (Neoproterozoic-Paleoproterozoic, South Africa). *South African Journal of Geology* 109, 23-54.
- Scott, C., Lyons, T.W., Bekker, A., Shen, Y., Poulton, S.W., Chu, X., Anbar, A.D., 2008. Tracing the stepwise oxygenation of the Proterozoic ocean. *Nature* 452, 456-459.
- Scott, C.T., Bekker, A., Reinhard, C.T., Schnetger, B., Krapež, B., Rumble III, D., Lyons, T.W., 2011. Late Archean euxinic conditions before the rise of atmospheric oxygen. *Geology* 39, 119-122.
- Siebert, C., McManus, J., Bice, A., Poulson, R., Berelson, W.M., 2006. Molybdenum isotope signatures in continental margin sediments. *Earth and Planetary Science Letters* 241, 723-733.
- Slotznick, S.P., Eiler, J.M., Fischer, W.W., 2018. The effects of metamorphism on iron mineralogy and the iron speciation proxy. *Geochimica et Cosmochimica Acta* 224, 96-115.
- Sossi, P.A., Eggins, S.M., Nesbitt, R.W., Nebel, O., Hergt, J.M., Campbell, I.H., O'Neill, H.S.C., Van Kranendonk, M., Davies, D.R., 2016. Petrogenesis and geochemistry of Archean komatiites. *Journal of Petrology* 57, 147-184.
- Stüeken, E.E., Buick, R., Anbar, A.D., 2015. Selenium isotopes support free  $\text{O}_2$  in the latest Archean. *Geology* 43, 259-262.

- Sumner, D.Y., Bowring, S.A., 1996. U-Pb geochronologic constraints on deposition of the Campbellrand Subgroup, Transvaal Supergroup, South Africa. *Precambrian Research* 79, 25-35.
- Sumner, D.Y., Hawes, I., Mackey, T.J., Jungblut, A.D., Doran, P.T., 2015. Antarctic microbial mats: a modern analog for Archean lacustrine oxygen oases. *Geology* 43, 887-890.
- Tissot, F.L.H., Chen, C., Go, B.M., Naziemiec, M., Healy, G., Bekker, A., Swart, P.K., Dauphas, N., 2018. Controls of eustasy and diagenesis on the  $^{238}\text{U}/^{235}\text{U}$  of carbonates and evolution of the seawater ( $^{234}\text{U}/^{238}\text{U}$ ) during the last 1.4 Myr. *Geochimica et Cosmochimica Acta* 242, 233-265.
- Trendall, A.F., Nelson, D.R., De Laeter, J.R., Hassler, S.W., 1998. Precise zircon U-Pb ages from the Marra Mamba iron formation and Wittenoom Formation, Hamersley Group, Western Australia. *Australian Journal of Earth Sciences* 45, 137-142.
- Trendall, A.F., Compston, W., Nelson, D.R., De Laeter, J.R., Bennett, V.C., 2004. SHRIMP zircon ages constraining the depositional chronology of the Hamersley Group, Western Australia. *Australian Journal of Earth Sciences* 51, 621-644.
- Voegelin, A.R., Nägler, T.F., Beukes, N.J., Lacassie, J.P., 2010. Molybdenum isotopes in late Archean carbonate rocks: implications for early Earth oxygenation. *Precambrian Research* 182, 70-82.
- Voegelin, A.R., Pettke, T., Greber, N.D., von Niederhäusern, B., Nägler, T.F., 2014. Magma differentiation fractionates Mo isotope ratios: Evidence from the Kos Plateau Tuff (Aegean Arc). *Lithos* 190-191, 440-448.
- Wasylenki, L.E., Rolfe, B.A., Weeks, C.L., Spiro, T.G., Anbar, A.D., 2008. Experimental investigation of the effects of temperature and ionic strength on Mo isotope fractionation during adsorption to manganese oxides. *Geochimica et Cosmochimica Acta* 72, 5997-6005.
- Wedepohl, H., 1995. The composition of the continental crust. *Geochimica et Cosmochimica Acta* 59, 1217-1239.
- Widdel, F., Schnell, S., Heising, S., Ehrenreich, A., Assmus, B., Schink, B., 1993. Ferrous iron oxidation by anoxygenic phototrophic bacteria, *Nature* 362, 834-836.
- Willbold, M., Elliot T., 2017. Molybdenum isotope variations in magmatic rocks. *Chemical Geology* 449, 253-268.
- Wille, M., Kramers, J.D., Nägler, T.F., Beukes, N.J., Schröder, S., Meisel, T., Lacassie, J.P., Voegelin, A.R., 2007. Evidence for a gradual rise of oxygen between 2.6 and 2.5 Ga from Mo isotopes and Re-PGE signatures in shales. *Geochimica et Cosmochimica Acta* 71, 2417-2435.
- Zahnle, K., Claire, M., Catling, D., 2006. The loss of mass-independent fractionation in sulfur due to a Palaeoproterozoic collapse of atmospheric methane. *Geobiology* 4, 271-283.
- Zerkle, A.L., Claire, M.W., Domagal-Goldman, S.D., Farquhar, J., Poulton, S.W., 2012. A bistable organic-rich atmosphere on the Neoproterozoic Earth. *Nature Geoscience* 5, 359-363.

**Acknowledgements:**

This research was supported financially by the NSF Frontiers in Earth System Dynamics program award NSF EAR-1338810 (C.M.O., T.W.L., and A.D.A.), the Natural Sciences and Engineering Research Council of Canada (NSERC) Discovery Grant RGPIN-435930 (B.K.), and by an ASU NASA Space Grant (C.M.O.). This material is based upon work supported by the National Science Foundation Graduate Research Fellowship Program under Grant No. 026257-001 (C.M.O.). Any opinions, findings, and conclusions or recommendations expressed in this material are those of the authors and do not necessarily reflect the views of the National Science Foundation.

**Figures and Figure Captions:**

**Figure 1. Generalized stratigraphic columns of the drill cores targeted in this study.** Intervals targeted in this section are signified by red rectangles to the left of the unit names. For more detailed stratigraphy of these cores, see subsequent figures or refer to Schröder et al. 2006 (GKP01 and GKF01), Anbar et al. 2007 (upper ABDP9), Kurzweil et al. 2015 (lower ABDP9), and Koehler et al. 2018 (AIDP2 and AIDP3). Available geochronological constraints and stratigraphic correlations have been included (see legend box for references). Some unit names have been abbreviated to conserve space: M.M. = Marra Mamba, Br. Fm. = Brockman Iron Formation, L. Fm. = Lokammona Formation, K. Mbr. = Kamden Member, K. Fm. = Kuruman Iron Formation, B. Fm. = Boomplaas Formation.

**Figure 2. Geochemistry of shales from the Jeerinah Formation preserved in drill cores AIDP2 (top) and AIDP3 (bottom).** Stratigraphy is modified from Koehler et al. (2018) and iron speciation and Mo concentration data are from Olson et al. (2019). Purple circles signify shale samples deposited, according to Fe speciation, under euxinic conditions ( $\text{FeHR}/\text{FeT} \geq 0.38$  and  $\text{FePy}/\text{FeHR} \geq 0.80$  [Poulton and Canfield 2011]). Dashed lines signify relaxed thresholds for anoxic and euxinic conditions ( $\text{FeHR}/\text{FeT} \geq 0.22$  and  $\text{FePy}/\text{FeHR} \geq 0.70$  [Poulton and Canfield 2011]). White circles signify shale samples deposited under non-euxinic conditions. Shale samples represented with an “x” have no accompanying Fe speciation data. All  $\delta^{98}\text{Mo}$  are bulk-rock values.

**Figure 3. Geochemistry of shales from the Wittenoom and Mt. Sylvia Formations preserved in drill core ABDP9.** The lone purple circle signifies the only shale sample deposited, according to Fe speciation,

under euxinic conditions ( $\text{FeHR}/\text{FeT} \geq 0.38$  and  $\text{FePy}/\text{FeHR} \geq 0.80$  [Poulton and Canfield 2011]). Dashed lines signify relaxed thresholds for anoxic and euxinic conditions ( $\text{FeHR}/\text{FeT} \geq 0.22$  and  $\text{FePy}/\text{FeHR} \geq 0.70$  [Poulton and Canfield 2011]). White circles signify shale samples deposited under non-euxinic conditions. Shale samples represented with an “x” have no accompanying Fe speciation data. All  $\delta^{98}\text{Mo}$  are bulk-rock values.

**Figure 4. Geochemistry of shales from the Klein Naute and Nauga Formations preserved in drill core GKP01.** Stratigraphy, iron speciation, and the bulk of the Mo concentration data is from Kendall et al. (2010). Purple circles signify shale samples deposited, according to Fe speciation, under euxinic conditions ( $\text{FeHR}/\text{FeT} \geq 0.38$  and  $\text{FePy}/\text{FeHR} \geq 0.80$  [Poulton and Canfield 2011]). Dashed lines signify relaxed thresholds for anoxic and euxinic conditions ( $\text{FeHR}/\text{FeT} \geq 0.22$  and  $\text{FePy}/\text{FeHR} \geq 0.70$  [Poulton and Canfield 2011]). White circles signify shale samples deposited under non-euxinic conditions. Shale samples represented by “x” have no accompanying Fe speciation data and, in some cases, are from Wille et al. (2007). Samples represented by “+” are carbonates measured in Voegelin et al. (2010). All  $\delta^{98}\text{Mo}$  are bulk-rock values.

**Figure 5. Geochemistry of shales from the Klein Naute and Nauga Formations preserved in drill core GKF01.** Stratigraphy, iron speciation, and the bulk of the Mo concentration data is from Kendall et al. (2010). Purple circles signify shale samples deposited, according to Fe speciation, under euxinic conditions ( $\text{FeHR}/\text{FeT} \geq 0.38$  and  $\text{FePy}/\text{FeHR} \geq 0.80$  [Poulton and Canfield 2011]). Dashed lines signify relaxed thresholds for anoxic and euxinic conditions ( $\text{FeHR}/\text{FeT} \geq 0.22$  and  $\text{FePy}/\text{FeHR} \geq 0.70$  [Poulton and Canfield 2011]). White circles signify shale samples deposited under non-euxinic conditions. Shale samples represented by “x” have no accompanying Fe speciation data. Samples represented by “+” are carbonates measured in Voegelin et al. (2010). See Figure 4 for a stratigraphic legend. All  $\delta^{98}\text{Mo}$  are bulk-rock values.

**Figure 6. A cross-plot of  $\delta^{98}\text{Mo}$  versus Mo/Al for all shales in our sample set.** The black line is a logarithmic trendline through the data ( $R^2 = 0.65$ ). This general trend may signify binary mixing between a light  $\delta^{98}\text{Mo}$  and low Mo/Al component (perhaps continental detritus) and a comparatively heavy  $\delta^{98}\text{Mo}$  and high Mo/Al component (perhaps a seawater-derived authigenic component). All  $\delta^{98}\text{Mo}$  are bulk-rock values.

**Figure 7. Cross-plots illustrating the magnitude of authigenic correction that is applied to our shale samples for a given detrital  $\delta^{98}\text{Mo}$  and Mo/Al value.** (upper panel) Magnitude of  $\delta^{98}\text{Mo}$  correction

(signified by  $\Delta^{98}\text{Mo}_{\text{authigenic-shale}}$ ) that is applied to our measured bulk-rock shale values assuming  $\text{Mo}/\text{Al} = 0.13$ , but with variable  $\delta^{98}\text{Mo}_{\text{detrital}}$ . (lower panel). Magnitude of correction that is applied to our measured bulk-rock shale values assuming  $\delta^{98}\text{Mo}_{\text{detrital}} = 0.25$ , but with variable  $\text{Mo}/\text{Al}_{\text{detrital}}$ . Because the authigenic corrections become highly dependent on  $\delta^{98}\text{Mo}_{\text{detrital}}$  and/or  $\text{Mo}/\text{Al}_{\text{detrital}}$  above  $f_{\text{detrital}} \sim 0.6$ , we have chosen to not utilize for interpretation  $\delta^{98}\text{Mo}_{\text{authigenic}}$  from shales with  $f_{\text{detrital}} \geq 0.6$ .

**Figure 8. Shale Re and Mo abundance cross plot from the roughly coeval Nauga (Kaapvaal Craton) and Wittenoom/Mt. Sylvia (Pilbara Craton) Formations.** Trace metal abundance data from the Nauga Formation is from Kendall et al. (2010) and is interpreted as evidence for locally suboxic conditions during original deposition. Our new data from the Wittenoom and Mt. Sylvia Formations does not possess the same trend and therefore was probably not deposited under the same local redox conditions.

**Figure 9. Updated late-Archean (~2.70 Ga to 2.50 Ga) sedimentary Mo isotope record.** See Fig. 1 for geochronological references. An authigenic correction has been applied to the majority of data from this study (see **Section 5.1.**). Purple circles signify shale samples deposited, according to Fe speciation, under euxinic conditions ( $\text{FeHR}/\text{FeT} \geq 0.38$  and  $\text{FePy}/\text{FeHR} \geq 0.80$  [Poulton and Canfield 2011]). White circles signify shale samples deposited under non-euxinic conditions. Shale samples represented by “x” have no accompanying Fe speciation data. Samples represented by diamonds are carbonates, and squares signify Mo isotope data from iron formations. The brown rectangle signifies our estimated late-Archean detrital  $\delta^{98}\text{Mo}$  value ( $\sim 0.25\%$ ; see **Section 5.1.**). Data sources are as follows: Wille et al. (2007), Voegelin et al. (2010), Duan et al. (2010), Kurzweil et al. (2015), Eroglu et al. (2015), Ostrander et al. (2019a), and this study.



# Pilbara Craton, Western Australia

# Kaapvaal Craton, South Africa

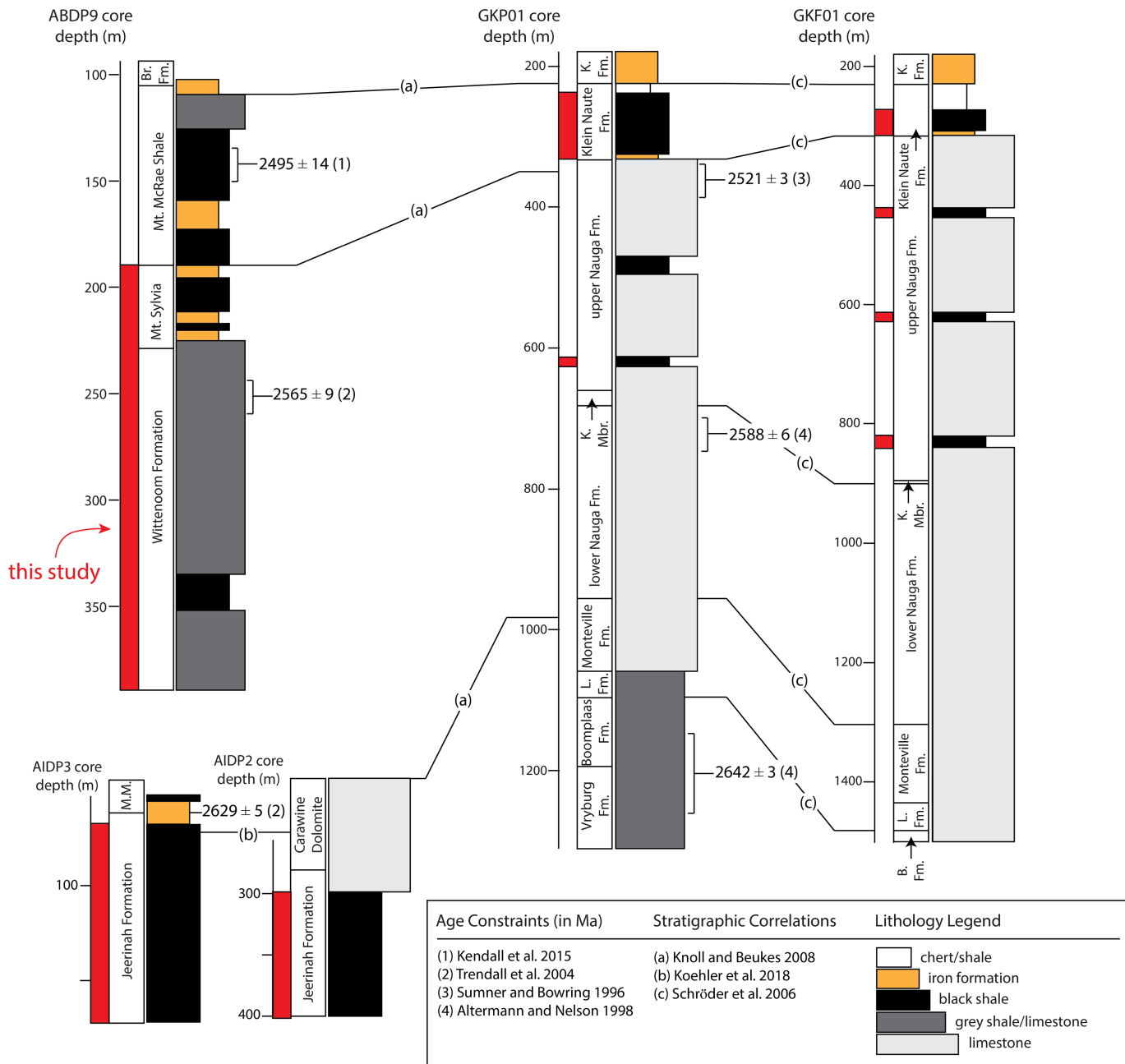


Figure 1

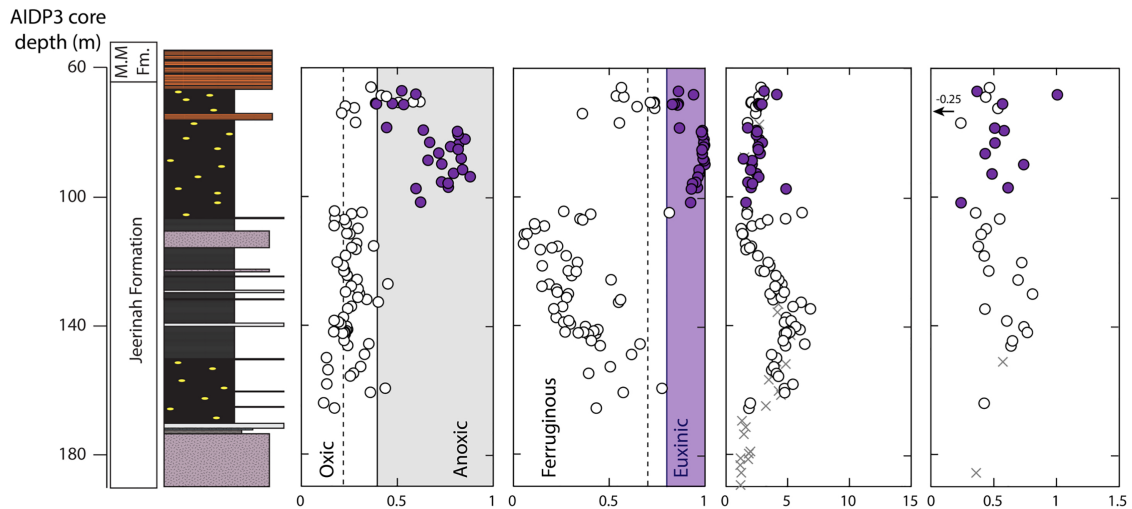
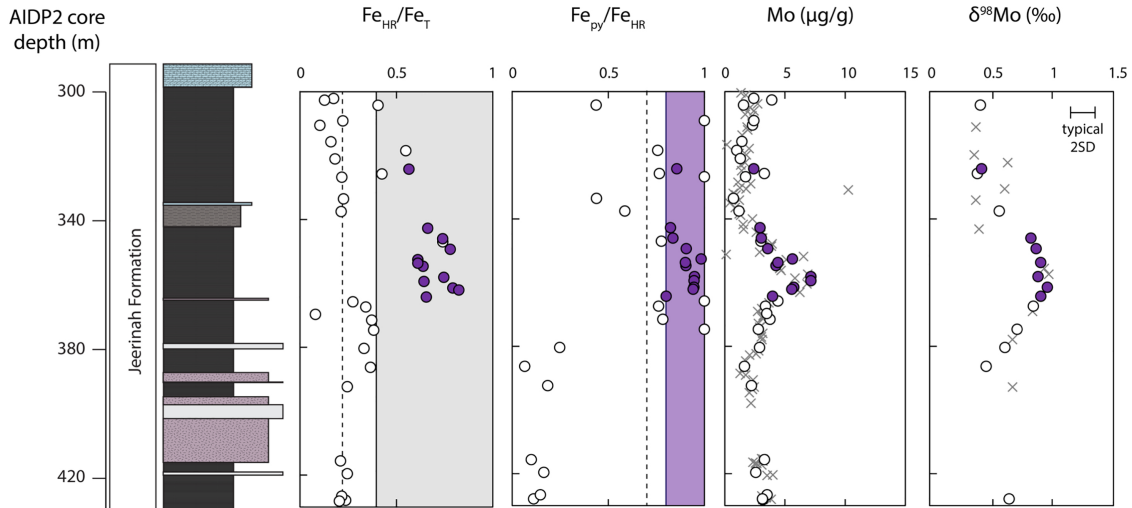
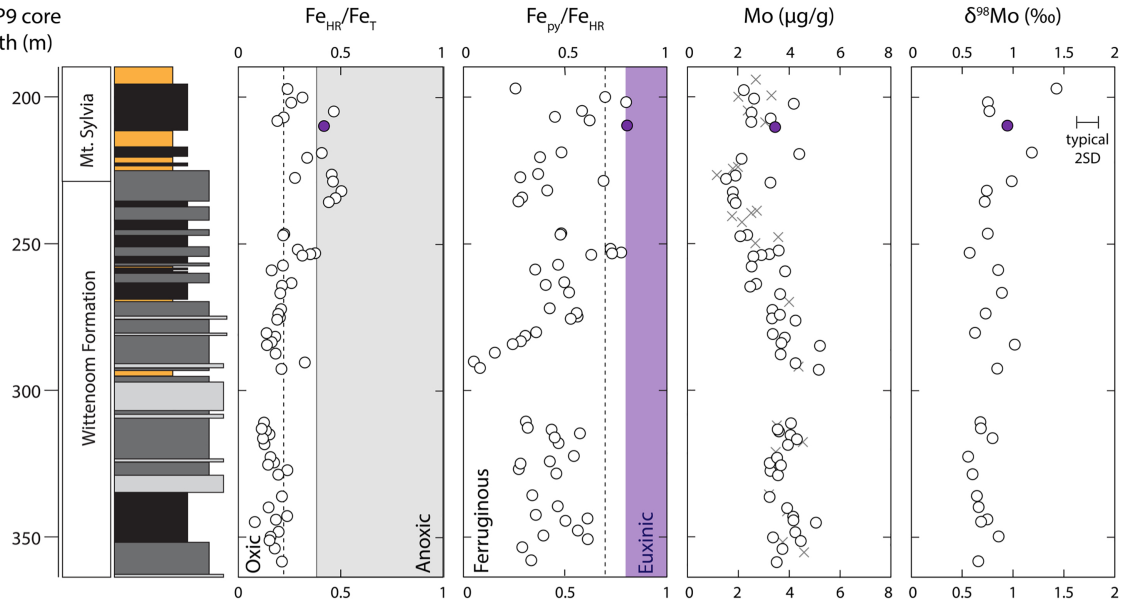


Figure 2

ABDP9 core depth (m)







 BIF (siderite)     grey carbonate/marl couplets or clastic carbonate     organic rich marl     black laminated shale

Figure 3

GKP01 core depth (m)

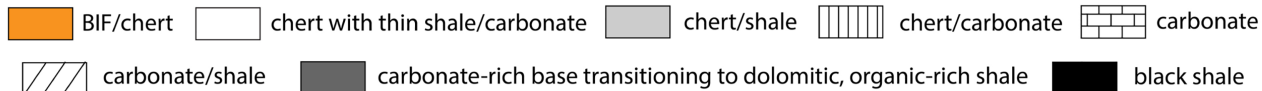
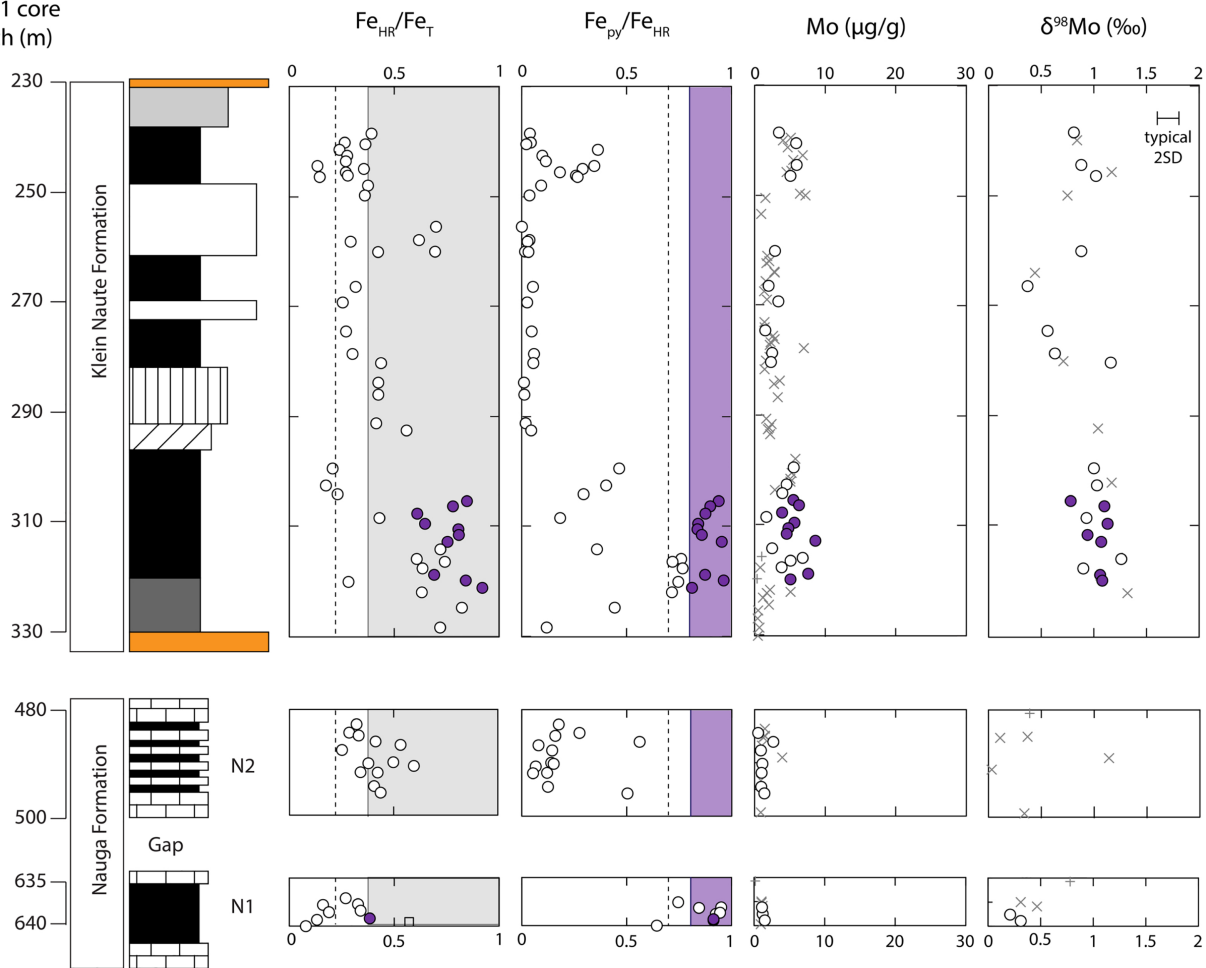


Figure 4

GKF01 core  
depth (m)

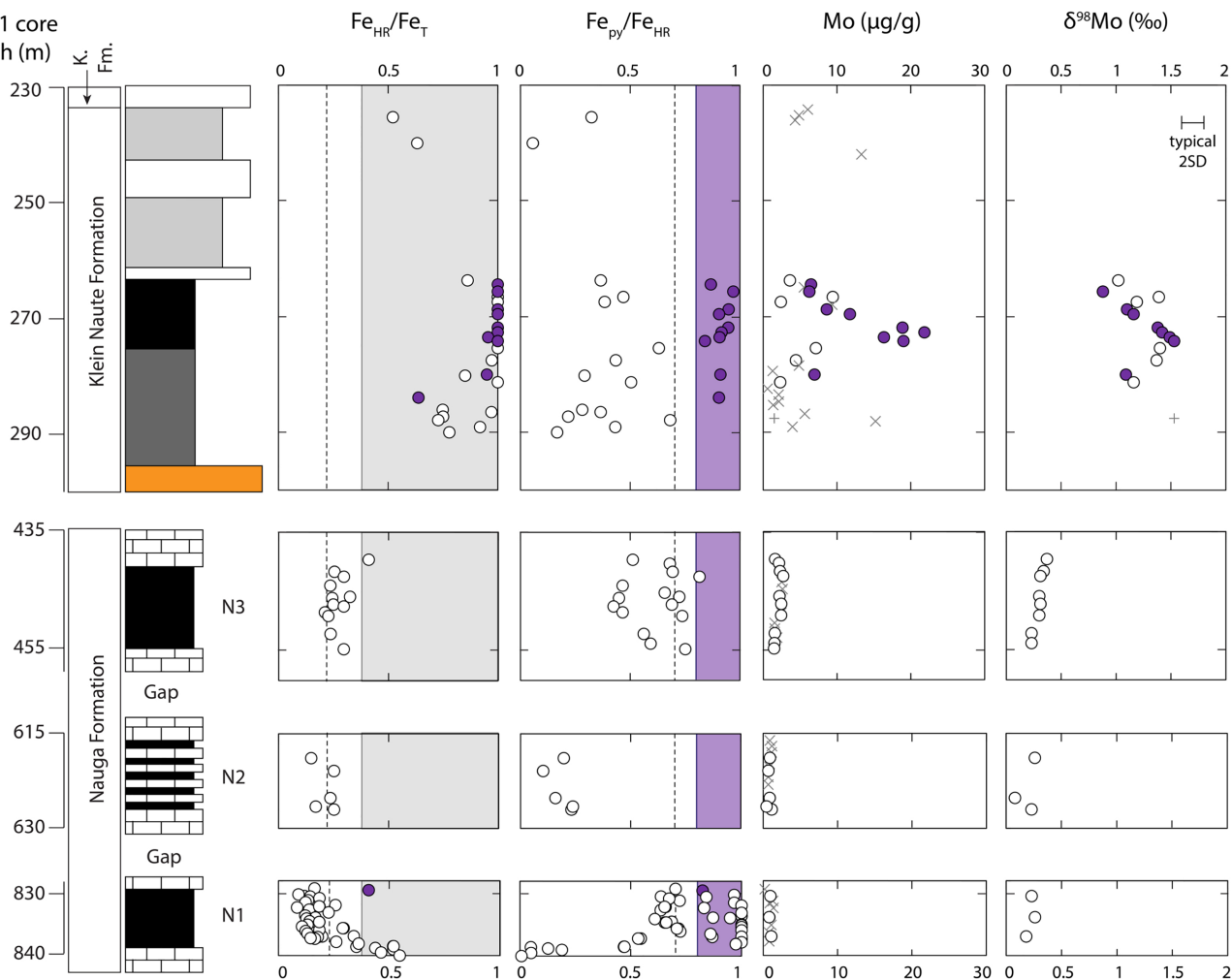


Figure 5

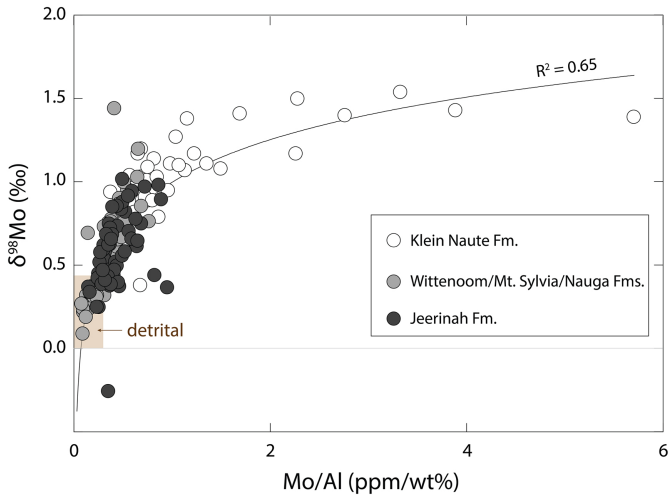


Figure 6



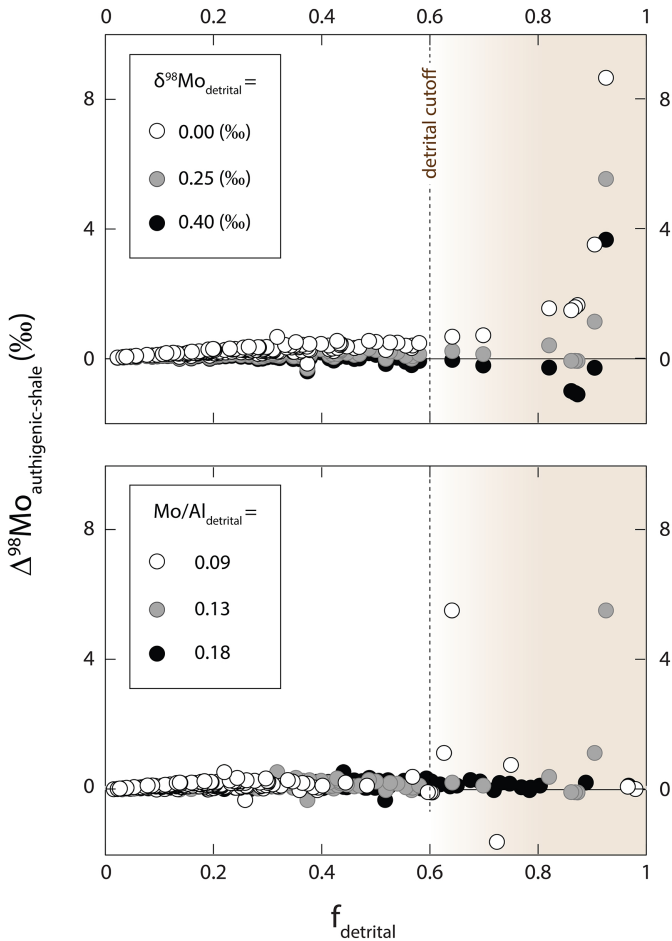


Figure 7

○ Nauga Formation  
(N2 and N3)

● Wittenoam and  
Mt. Sylvania Formations

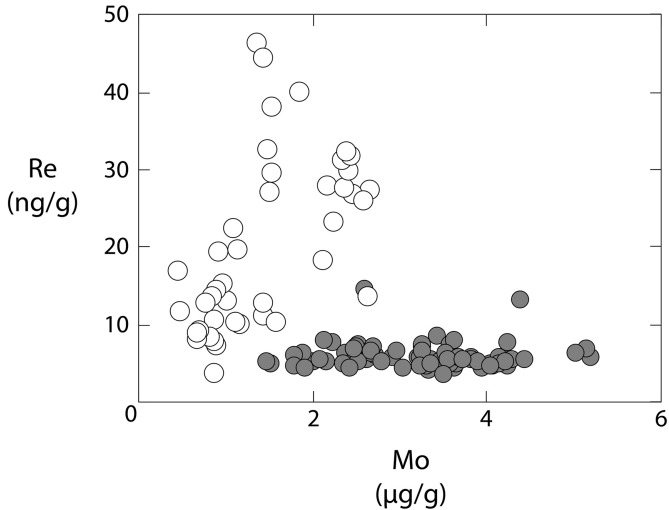
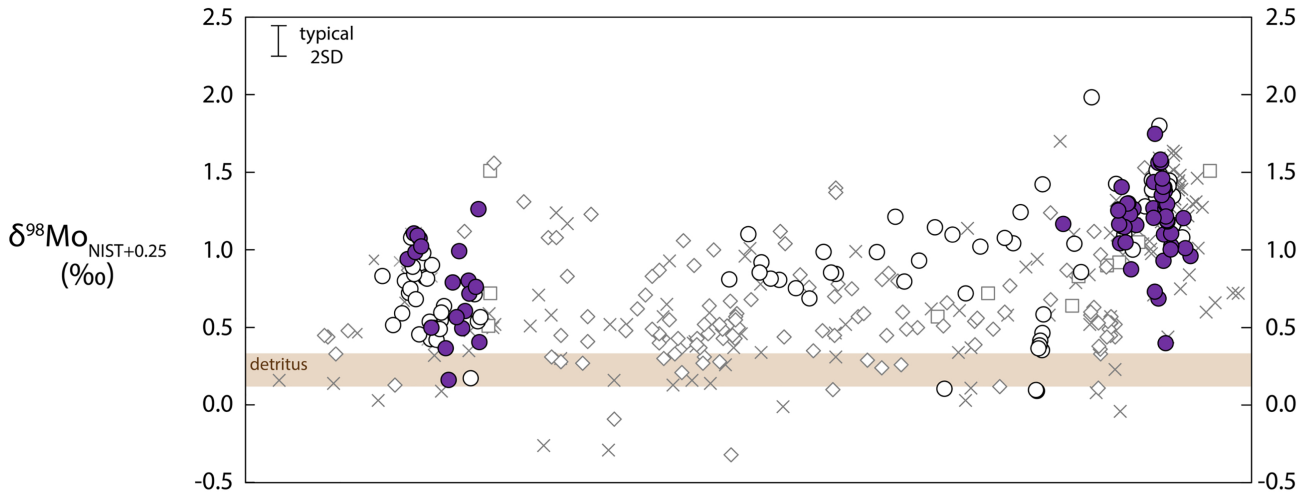
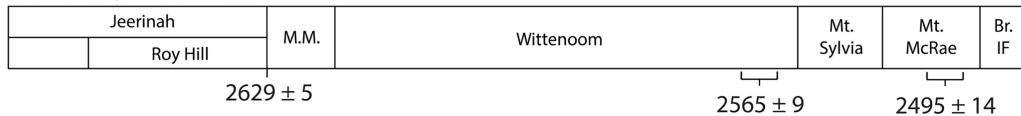


Figure 8



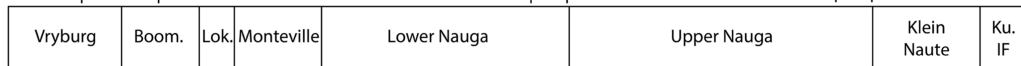
Pilbara Craton, Western Australia



$2642 \pm 3$  Ma

$2588 \pm 6$

$2521 \pm 3$



Kaapvaal Craton, South Africa

Figure 9